Geochemistry Geophysics Geosystems G3

Article
Volume 14, Number 3
28 March 2013
doi:10.1002/ggge.20068
ISSN: 1525-2027

Published by AGU and the Geochemical Society

Formation of thick stratiform Fe-Ti oxide layers in layered intrusion and frequent replenishment of fractionated mafic magma: Evidence from the Panzhihua intrusion, SW China

Xie-Yan Song, Hua-Wen Qi, Rui-Zhong Hu, Lie-Meng Chen, and Song-Yue Yu
State Key Laboratory of Ore Deposit Geochemistry, Institute of Geochemistry, Chinese Academy of Sciences, 46th Guanshui Road, Guiyang, China (songxieyan@vip.gyig.ac.cn;)

Jia-Fei Zhang
Pangang Group Company Ltd., Sichuan, China

[1] The Panzhihua intrusion is one of the largest layered intrusions that hosts huge stratiform Fe-Ti oxide layers in the central part of the Emeishan large igneous province, SW China. Up to 60 m thick stratiform massive Fe-Ti oxide layers containing ~85 modal% of magnetite and ilmenite and overlying magnetite gabbro compose cyclic units of the Lower Zone of the intrusion. The cyclic units of the Middle Zone consist of magnetite gabbro and overlying gabbro. In these cyclic units, contents of Fe_2O_3(t), TiO_2 and Cr and Fe^{3+}/Ti^{4+} ratio of the rocks decrease upward, Cr content of magnetite and forsterite percentage of olivine decrease as well. The Upper Zone consists of apatite gabbro characterized by enrichment of incompatible elements (e.g., 12–18 ppm La, 20–28 ppm Y) and increasing of Fe^{3+}/Ti^{4+} ratio (from 1.3 to 2.3) upward. These features indicate that the Panzhihua intrusion was repeatedly recharged by more primitive magma and evolved magmas had been extracted. Calculations using MELTS indicate that extensive fractionation of olivine and clinopyroxene in deep level resulted in increasing Fe and Ti contents in the magma. When these Fe-Ti-enriched magmas were emplaced along the base of the Panzhihua intrusion, Fe-Ti oxides became an early crystallization phase, leading to a residual magma of lower density. We propose that the unusually thick stratiform Fe-Ti oxide layers resulted from coupling of gravity settling and sorting of the crystallized Fe-Ti oxides from Fe-Ti-enriched magmas and frequent magma replenishment along the floor of the magma chamber.

Components: 11,300 words, 12 figures.

Keywords: Fe-Ti oxide accumulation; layered intrusion; magma replenishment; open magma system; Panzhihua.

Index Terms: 3618 Magma chamber processes: Magma chamber processes (1036); 3610 Geochemical modeling: Geochemical modeling (1009, 8410); 8410 Geochemical modeling: Geochemical modeling (1009, 3610).

Received 22 October 2012; **Revised** 11 January 2013; **Accepted** 11 January 2013; **Published** 28 March 2013.

Song, X.-Y., H.-W. Qi, R.-Z. Hu, L.-M. Chen, S.-Y. Yu, and J.-F. Zhang (2013), Formation of thick stratiform Fe-Ti oxide layers in layered intrusion and frequent replenishment of fractionated mafic magma: Evidence from the Panzhihua intrusion, SW China, *Geochem. Geophys. Geosyst.*, *14*, 712–732, doi:10.1002/ggge.20068.

1. Introduction

[2] Layered mafic intrusions and their stratiform Fe-Ti oxide and chromitite layers are very significant for understanding the chemical processes and physical mechanisms of magmatic evolution in a large, sheet-like magma chamber [e.g., *Wager and Brown*, 1967; *Irvine and Sharpe*, 1986; and references therein]. It is widely accepted that the formation of chromitite layers in layered intrusions is associated with fractional crystallization or magma mixing [*Irvine*, 1977; *Eales*, 2000; *Mondal and Mathez*, 2007; *Voordouw et al*., 2009; *Naldrett et al*., 2012]. However, although the Fe-Ti oxide layers in layered intrusions are commonly interpreted as accumulations of Fe-Ti oxides in late magmatic fractionation stages [*Wager and Brown*, 1967; *Klemm et al*., 1985], some researchers have argued that they are associated with a Fe-rich immiscible liquid segregated from mafic magma [*Bateman*, 1951; *Reynolds*, 1985; *von Gruenewaldt*, 1993; *Zhou et al*., 2005]; magma addition and/or mixing [*Harney et al*., 1990]; change in oxygen content [*Klemm et al*., 1985]; or change in pressure [*Cawthorn and McCarthy*, 1980].

[3] In the central part of the Emeishan large igneous province (ELIP), SW China, the Permian mafic-ultramafic layered intrusions are associated with a Permian mantle plume [*Zhou et al*., 2002; *Song et al*., 2005a, 2005b; and references therein] (Figure 1). Unusually thick stratiform massive Fe-Ti oxide layers (up to 60 m thick) and magnetite gabbro (up to 200 m thick) occur in the lower portions of the layered intrusions [*Panxi Geological Unit*, 1984]. In the Sept Iles layered intrusion, Canada, the third largest layered intrusion in the wolrd, very thick Fe-Ti oxide-rich troctolites occur in the Layered Series in lower portion of the intrusion, whereas thicknesses of the massive oxide layers within the Layered Series are up to 16 m [*Namur et al*., 2010]. In contrast, Fe-Ti oxides appear as cumulus phases in the upper part of the Bushveld Complex and the middle parts of the Skaergaard intrusion because of their more primitive parental magmas [*Wager and Brown*, 1967; *Cawthorn and Molyneux*, 1986; *Tegner et al*., 2006; *Nielsen*, 2004]. The formation of such thick stratiform Fe-Ti oxide layers in the Emeishan LIP layered intrusions have simply been attributed to gravity accumulation of Fe-Ti oxides during fractionation [*Zhang and Luo*, 1988; *Pang et al*., 2008a, 2008b]. *Ganino et al*. [2008] proposed that interaction with the dolomite that underlies the Panzhihia intrusion increased the oxygen fugacity of the magma and promoted magnetite crystallization. The previous studies have paid inadequate attention to the potentially significant role of dynamic processes such as fractionation at deep level, fractionated magma injection, and crystallization along the base of the magma chamber for the formation of the thick massive stratiform Fe-Ti oxide layers.

[4] This paper provides detailed petrographic and compositional data for the rocks and minerals, and trace elements and Sr-Nd isotopes of the massive oxides and gabbros systematically collected from the base to the top of the Panzhihua intrusion at three locations. This study leads us to propose that the thick stratiform layers of massive Fe-Ti oxide and magnetite gabbro in the Lower and Middle zones of the Panzhihua intrusion resulted from coupling of gravity settling and sorting of the Fe-Ti oxides crystallized from Fe-Ti-enriched mafic magmas frequently replenished from deep level along the floor of the magma chamber. Fe-Ti oxides are the early crystallizing phases from the Fe-Ti-enriched mafic magmas.

2. Geological Background

[5] Southwest China comprises the Yangtze and Cathaysian blocks in the east and the Tibetan Plateau in the west (Figure 1). The Yangtze Block contains a Proterozoic metamorphic basement, a middle sequence of Paleozoic marine sedimentary strata, and a Mesozoic and Cenozoic terrestrial sedimentary cover. In the western Yangtze Block, the early Late Permian Emeishan flood basalts cover an area of more than 5×10^5 km^2, which extend southward into northern Vietnam, and associated intrusions compose the ELIP [*Xu et al*., 2001; *Song et al*., 2001, 2004]. The Emeishan basalts have been divided into high-Ti and low-Ti basalts. The high-Ti basalts were derived from a garnet-stable mantle source and experienced weak crustal contamination, whereas the low-Ti basalts were produced via partial melting of a shallower mantle source and experienced variable degrees of crustal contamination [*Xu et al*., 2001; *Xiao et al*., 2004; *Song et al*., 2009]. The associated intrusions include large and small layered mafic-ultramafic intrusions, and syenite and A-type granite [*Shellnutt and Zhou*, 2007; *Zhong et al*., 2007, 2009]. The mafic-ultramafic intrusions have been dated at 258–263 Ma using the sensitive high-resolution ion microprobe (SHRIMP) technique on zircon crystals separated from gabbros [*Zhou et al*., 2002, 2005; *Zhong and Zhu*, 2006]. Trace element compositions and Sr-Nd isotopes of the intrusive and extrusive rocks suggest that they were related to a mantle plume [*Chung and Jahn*, 1995;

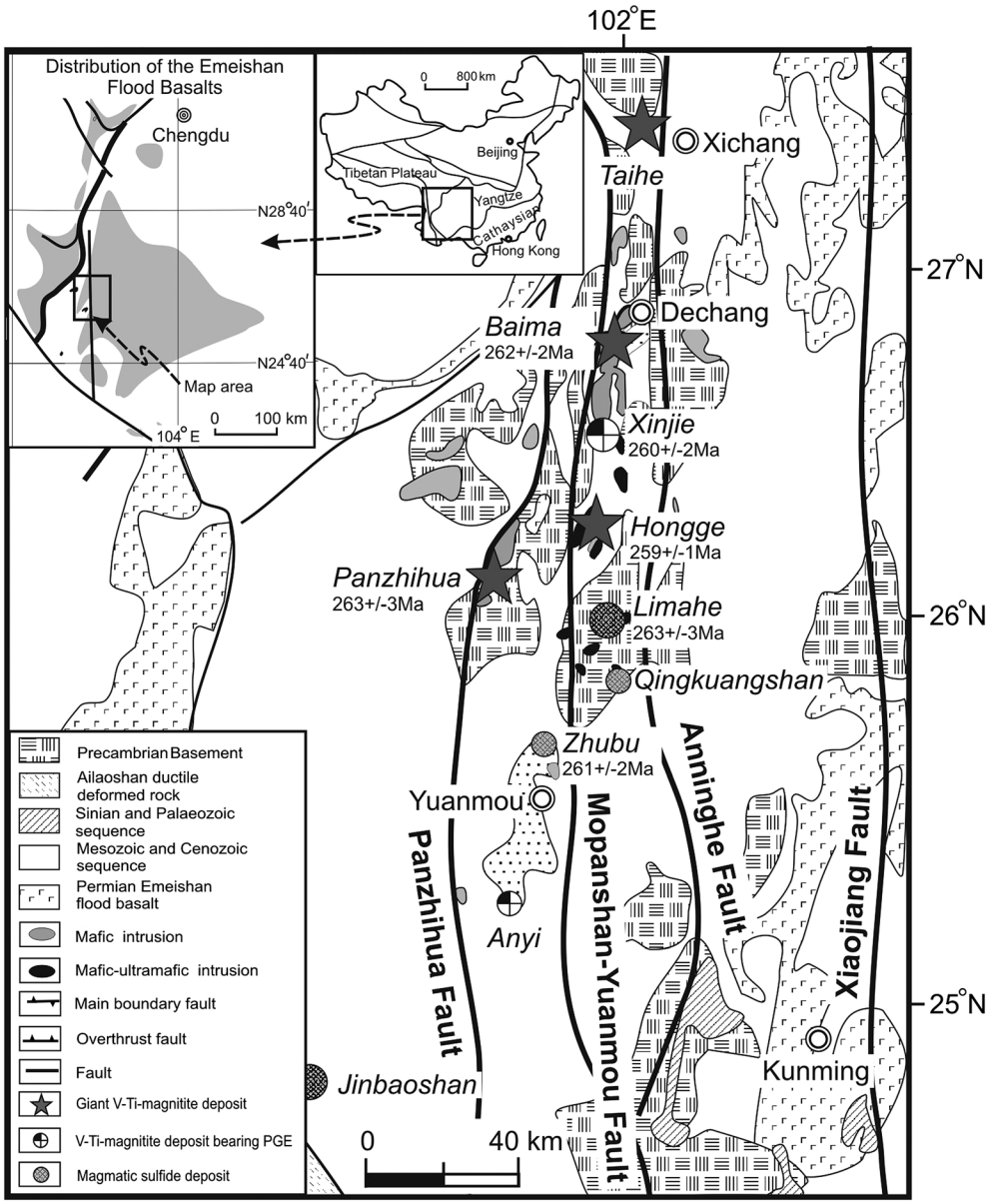

Figure 1. Regional geological map of the central Emeishan large igneous province, showing the distribution of the layered intrusions hosting Fe-Ti oxide deposits and the mafic-ultramafic bodies hosting Ni-Cu-(PGE) sulfide deposits (after *Geology and Mineral Resource Bureau of Sichuan Province* [1991]; *Panxi Geological Unit* [1984], and *Song et al*. [2008a]). Ages of the intrusions are from *Zhou et al*. [2002, 2005, 2008] and *Zhong and Zhu* [2006].

Xu et al., 2001; *Zhou et al*., 2002; *Zhang et al*., 2006; and references therein].

[6] Mafic and mafic-ultramafic layered intrusions occurring along N-S-trending Panzhihua Fault and Anninghe Fault emplaced in the Proterozoic and Paleozoic strata in the central ELIP (Figure 1) [*Panxi Geological Unit*, 1984; *Zhang and Luo*, 1988]. Some of them host Fe-Ti oxide deposits and a few of them contain both Fe-Ti oxide layers and PGE sulfide mineralization [*Zhong et al*., 2004; *Zhou et al*., 2008]. Exploration projects completed in the 1950s–1970s have indicated that total Fe-Ti-V reserves in more than 30 mafic-ultramafic intrusions are >10 billion tonnes ore with grades of 25–55wt% Fe, 4–13wt% Ti, and 0.1–0.45wt% V in the four largest deposits including Panzhihua, Hongge, Baima, and Taihe [*Panxi Geological Unit*, 1984]. Some relatively small mafic-ultramafic intrusions may contain economic or uneconomic sulfides (Figure 1) [*Song et al*., 2003, 2008a; *Zhou et al*., 2008].

[7] In the mafic layered intrusions, such as Panzhihua, Baima, and Taihe, the stratiform Fe-Ti oxide layers composed of massive oxides or magnetite gabbro are situated at the bases and lower parts of the intrusions (Figure 2). In the mafic-ultramafic layered intrusions, such as Hongge and Xinjie, consisting of olivine clinopyroxenite, clinopyroxenite, and gabbro from base to top, the Fe-Ti oxide layers not only occur in the basal parts of the layered gabbro, but are also present in the olivine clinopyroxenite and clinopyroxenite (Figure 2).

3. Stratigraphic Subdivision and Petrography of the Panzhihua Intrusion

[8] The NE-SW-striking Panzhihua layered intrusion is about 19 km long, dips northwest at angles ranging from 40° to 60°, and was emplaced into the Neoproterozoic dolomitic limestone, gneiss, and schist (Figure 3) [*Panxi Geological Unit*, 1984]. The intrusion has been divided into seven segments by a series of N-S-trending strike faults, including Zhujiabaobao, Lanjiahuoshan, Jianbaobao, Daomakan, Gongshan, Nongnongping, and Nalaqing from NE to SW (Figure 3). At the northwest end, a NE-SW-trending, steeply SE-dipping thrust fault juxtaposes the intrusion against Permian syenite and Triassic terrestrial clastic strata (Figure 3). This implies that the original thickness of the Panzhihua intrusion was >2000 m.

[9] The Panzhihua intrusion can be divided into the Marginal Zone and Lower, Middle, and Upper Zones from the base upward, based on textural features and cumulus mineral assemblages [*Panxi Geological Unit*, 1984]. The Marginal Zone mainly consists of fine-grained gabbro [*Zhou et al.*, 2005] (Figures 3 and 4). A series of stratiform Fe-Ti oxide ore layers are present in the Lower and Middle Zones, which are thick in the northern segments of the intrusion and thin southward (Figure 4).

3.1. Lower Zone

[10] According to our investigation, the Lower Zone includes five cyclic units (I to V). In the cyclic unit I, coarse-grained magnetite gabbro is overlain by gabbro. The gabbro consists of ~45 modal% subhedral plagioclase and ~40% clinopyroxene, and 10-15% Fe–Ti magnetite and ilmenite; poikilitic fine-grained olivine enclosed in clinopyroxene and interstitial hornblende are less than modal 10%. The Fe-Ti oxides increase gradually up to 60% toward the magnetite gabbro; consistently, silicate minerals decrease downward.

[11] The cyclic units II to V are remarkable by massive oxide layers at the bases, which are overlain by medium-grained magnetite gabbro and melanogabbro (Figure 4). The stratiform massive oxide layers at the bases of the cyclic units II and V are up to 40–60 m thick in Zhujiabaobao and Lanjiahuoshan

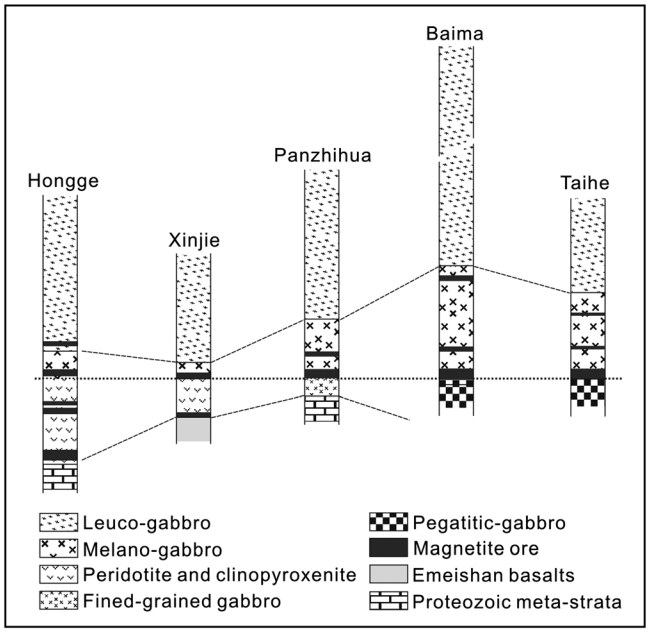

Figure 2. Petrographic columns of the layered intrusions hosting giant Fe-Ti oxide deposits in the central of the Emeishan large igneous province, showing the different positions of the Fe-Ti oxide layers in the mafic layered intrusions and the mafic-ultramafic intrusions (after *Panxi Geological Unit* [1984]).

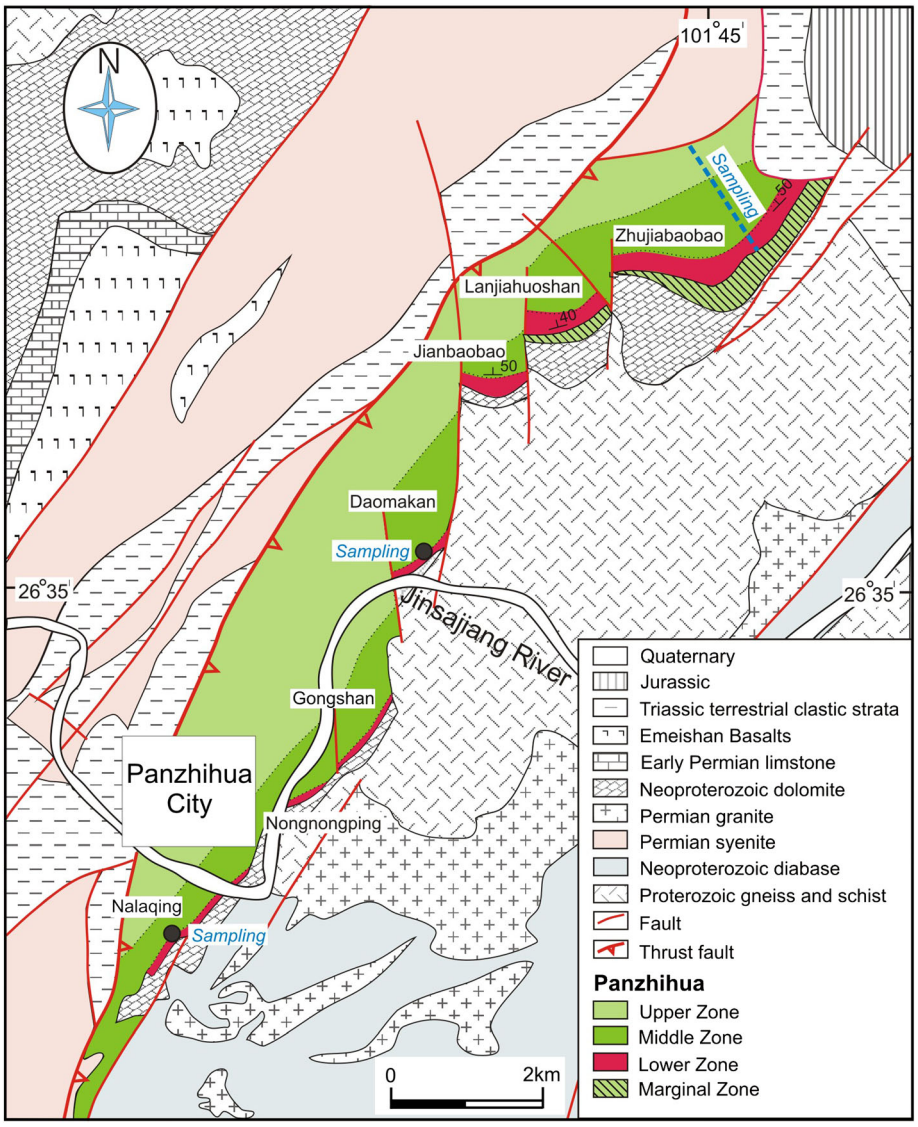

Figure 3. Geological map of the Panzhihua intrusion (after *Panxi Geological Unit* [1984]).

and evidently thin and disappear at Gongshan and Nalaqing [*Panxi Geological Unit*, 1984]. The cyclic units III and IV are also thin and disappear gradually toward the southwest (Figures 3 and 4).

[12] The massive oxide commonly contain >75 modal% magnetite, ~10% ilmenite, <10% silicate minerals (mainly clinopyroxene, plagioclase, and olivine), and 2–3 modal% interstitial pyrrhotite and minor pentlandite. A series of thin magnetite gabbro interlayers (10–20 cm thick but up to 30 cm) with sharp contacts occur within the massive oxide layers (Figure 5a). The magnetite gabbro interlayers consist of subhedral plagioclase and clinopyroxene, minor poikilitic olivine within clinopyroxene, and interstitial hornblende and <50% Fe-Ti oxides. The magnetite gabbros overlying the massive oxides commonly contain 20–30% clinopyroxene, <10% plagioclase, minor poikilitic olivine, 2–3% interstitial pyrrhotite and pentlandite, and as much as 40–60 modal% magnetite and ilmenite. The contents of oxides decrease gradually upward to <20%, and plagioclase increases up to 50% in the melanogabbro at the top of the cyclic units.

[13] In the Lower Zone, igneous foliation and lineation are shown by platy orientation of plagioclase and clinopyroxene in the magnetite gabbro and melanogabbro (Figure 5a). The most significant feature of the clinopyroxene crystals is their two sets of magnetite exsolution lamellae oriented parallel to the prismatic cleavages (Figure 5c).

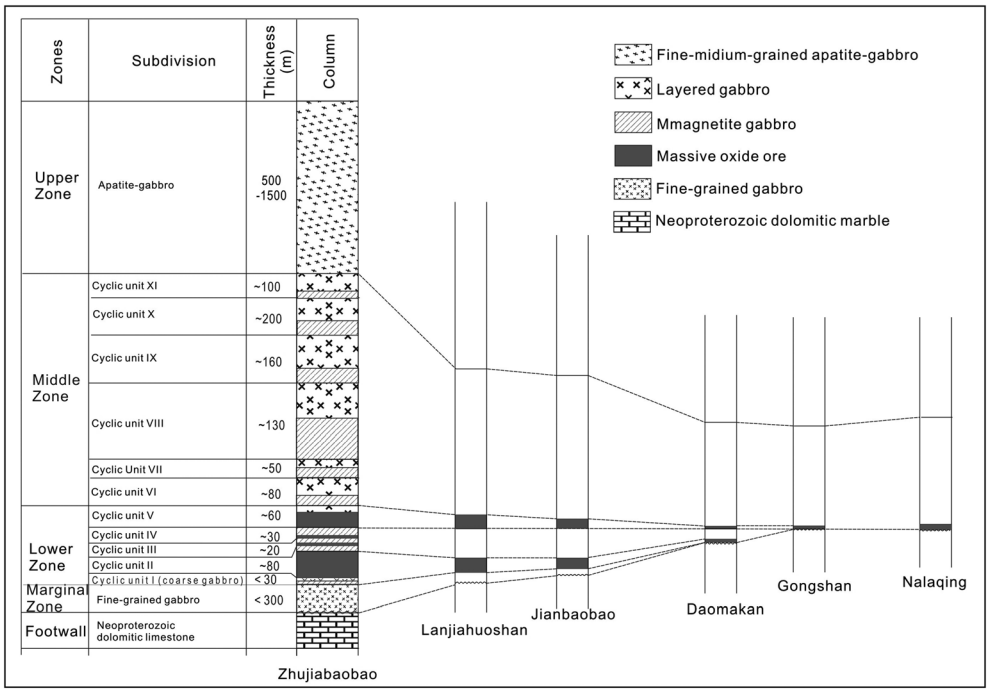

Figure 4. Petrographic columns of the Panzhihua intrusion (modified after *Panxi Geological Unit* [1984]).

3.2. Middle Zone

[14] The Middle Zone (equivalent to MZa unit of *Pang et al*. [2008a]) is more than 600 m thick at Zhujiabaobao and becomes thinner toward the southwest [*Panxi Geological Unit*, 1984, Figures 3 and 4]. Lithologic variations indicate six cyclic units in the Middle Zone, VI to XI from the base upward (Figure 4). Each cyclic unit comprises magnetite gabbro at the base and gabbro at the top as the Fe-Ti oxides gradually decrease upward (Figure 4). The base of each cyclic unit is marked by a sudden reappearance of significant modal Fe-Ti oxides. The silicate mineral assemblage of the magnetite gabbros are similar to those of the Lower Zone and commonly contain relatively lower Fe-Ti oxides (20–45%). The gabbros at the tops of these cyclic units contain 40–50% plagioclase, 30–40% clinopyroxene, and 10–20 oxides. Exsolution magnetite lamellae in the clinopyroxene crystals are also well developed in Middle Zone rocks. Rhythmic layering and planar foliation and lineation are shown by proportional variation between the contents of magnetite and clinopyroxen and plagioclase (Figures 5b and 5d).

3.3. Upper Zone

[15] The Upper Zone is marked by the appearance of cumulate apatite and is composed of medium- to fine-grained apatite gabbro. It is comparable with the MZb unit of *Pang et al*. [2008a]. Rhythmic layering and planar lineation are still shown by proportional variations of minerals and orientation of plagioclase and clinopyroxene in the Upper Zone, but the contents of Fe-Ti oxides at the bases of rhythmic layers are much lower than in the Lower and Middle Zones. The characteristic features of the apatite gabbro that are distinct from the gabbros in the Lower and Middle Zones are (1) high contents (up to 3–5 modal%) of apatite that are small hexagonal crystals and may be poikilitically enclosed by clinopyroxene and plagioclase (Figure 5e); (2) low Fe-Ti oxide contents, generally $<10\%$, rarely up to 15%; (3) rare magnetite exsolution lamellae in the clinopyroxene crystals; and (4) Fo percentages of olivine from 28 to 65 [*Pang et al*., 2009].

4. Sampling and Analytical Techniques

[16] In this study, 55 samples were collected from the Zhujiabaobao open-pit mine, where the Lower and Middle Zones are thick and very well exposed by extensive mining since the 1960s (Figure 3). The Marginal Zone was not sampled in this study. To avoid the effect of rhythmic modal layering on the investigation of large scale chemical variations, samples were collected from the lower parts of the modal layers. Twenty-eight samples were from the Daomakan segment, where only the Lower Zone is exposed by current mining. Thirty-seven samples

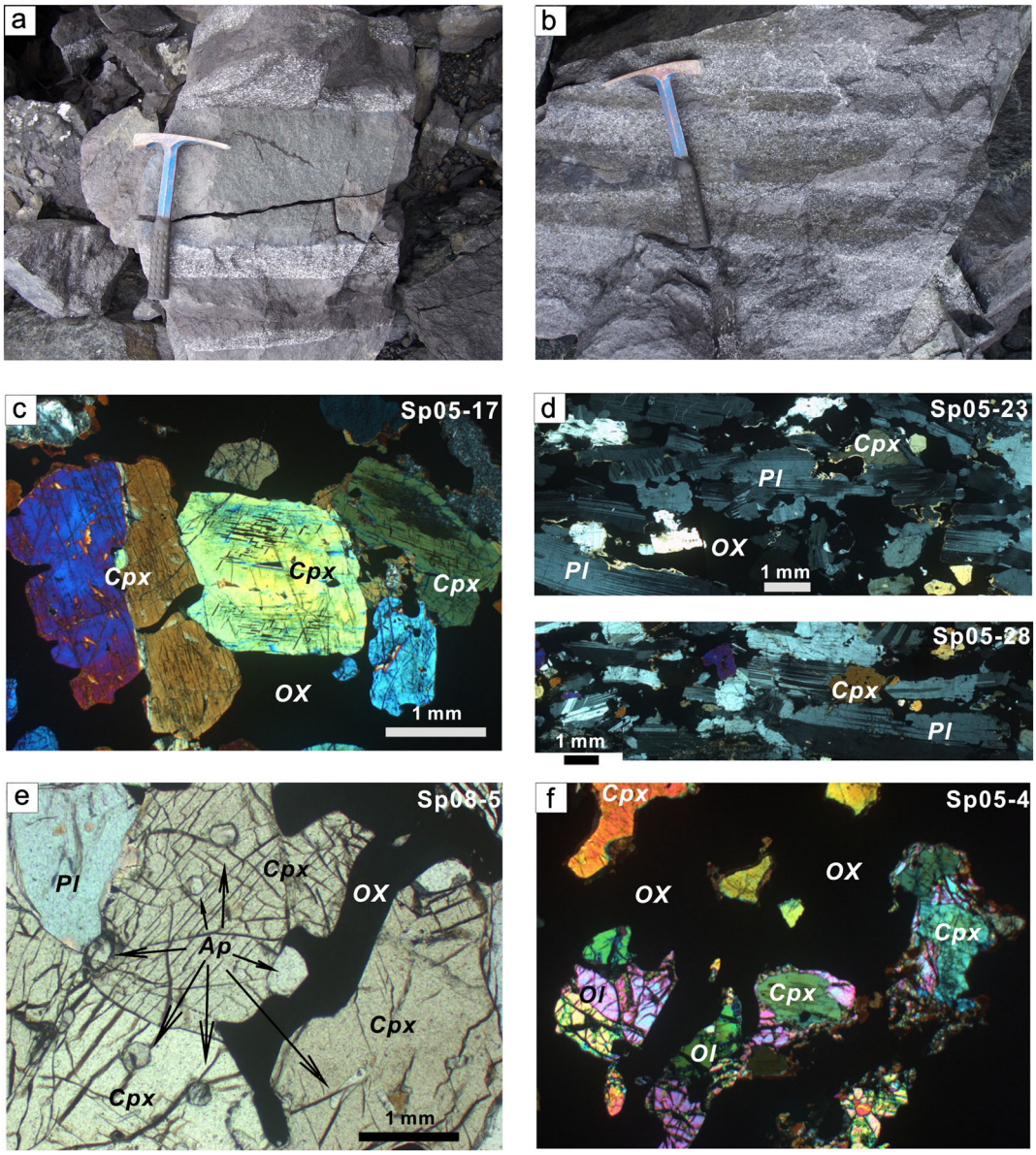

Figure 5. Lithological structures and textures of Panzhihua rocks. (a) Melanogabbro interlayers with sharp contacts in the massive Fe-Ti oxide layer of Lower Zone; (b) rhythmic layering in the Middle Zone with a base of magnetite gabbro and a top of gabbro; (c) two sets of exsolution magnetite lamellae oriented parallel to the prismatic cleavage in clinopyroxene grains; (d) planar foliation and lineation defined by orientation of plagioclase and clinopyroxene in the lower part of rhythmic layering; (e) fine, euhedral, hexagonal apatite grains poikilitically enclosed by Cpx and Pl in Upper Zone apatite gabbro; and (f) concave margins of the silicates in the massive oxides of the Lower Zone. Ol: olivine, Pl: plagioclase, Cpx: clinopyroxene, Ap: apatite, OX: magnetite and ilmenite.

in the Nalaqing segment were collected from exploration bore holes (ZK1212 and ZK1213), which cut through the Middle and Upper Zones.

[17] The samples were crushed in a jaw crusher, milled using a swing mill, and finely ground in an automatic agate mortar and pestle. Concentrations of oxides of the gabbros and Fe-Ti oxide ores were obtained at the Analytical Centre of the Metallogenic Geology Bureau of Southwestern China, Chengdu. For the major elements, SiO_2 and H_2O were determined by gravimetric methods; TiO_2 and P_2O_5 by spectrophotometry; Al_2O_3, Fe_2O_3, FeO, and CO_2 by titrimetry; and MnO, MgO, CaO, Na_2O, and K_2O by atomic absorption spectrometry. Contents of FeO were analyzed by titrimetry method after drying the sample at $<105^{\circ}C$ and Fe_2O_3 is obtained by subtracting FeO from total Fe. The analytical

uncertainty is usually <5% except for H_2O and CO_2. Trace elements, including rare earth element (REE), were analyzed using a Perkin-Elmer EIAN DRC II ICP-MS at the Institute of Geochemistry (Guiyang), Chinese Academy of Sciences. Fifty milligrams of powder for each sample was dissolved, in stainless steel bombs, under 200 °C for 12 hours, using the method described by *Liang and Gregoire*, 2000 and 500 mg/ml Rh was used as an internal standard. The nebulized solutions were analyzed using a VG Plasma-Quad Excell ICP-MS. We used standard additions, pure elemental standards for external calibration, and standards MSAN, OU-6, AMH-1, GBPG-1 as reference materials. Accuracy and precision of the ICP-MS analyses are estimated to be better than 5%. Major oxides and trace element analyses of the samples are listed in Table S1 in the Supporting Information.[1]

[18] Compositions of olivine and magnetite were determined by wavelength-dispersive X-ray using an EPMA-1600 electron microprobe at the State Key Laboratory of Ore Deposit Geochemistry, Institute of Geochemistry, Chinese Academy of Sciences. Beam size is 5 μm, beam current is 25 nA, and acceleration voltage is 25 kV. Both natural and synthetic standards were used for calibration. Contents of V_2O_3 were determined by energy disperse spectrum. Major oxide compositions of olivine and magnetite are listed in Table S2.

[19] Sr-Nd isotopic analyses were completed using a Finnegan MAT-261 multicollector mass spectrometer at China University of Geosciences (Wuhan). The measured $^{87}Sr/^{68}Sr$ and $^{143}Nd/^{144}Nd$ values were normalized to $^{86}Sr/^{88}Sr = 0.1194$ and $^{146}Nd/^{144}Nd = 0.7219$, respectively. During the period of analysis, the NBS987 standard and the La Jolla standard yielded $^{87}Sr/^{86}Sr = 0.71025 \pm 4(2\sigma)$ and $^{143}Nd/^{144}Nd = 0.511853 \pm 9(2\sigma)$, respectively. Total procedural Sr and Nd blanks are <1 ng and <50 pg, respectively. The detailed analytical procedures for Sr and Nd isotopes are given by *Zhang et al*. [1996]. The Sr-Nd isotope values of the Panzhihua rocks are listed in Table S3.

5. Results

5.1. Chemostratigraphic Variation

[20] In the cyclic units of the Lower Zone (except cyclic unit IV) at Zhujiabaobao, Fe_2O_3(t) and TiO_2 as well as $Al_2O_3/(K_2O + Na_2O)$ and Fe^{3+}/Ti^{4+} of whole-rock decrease regularly from the base to the top (Figure 6a), in concert with a clear upward increase of SiO_2 and Al_2O_3 (Table S1). The massive oxides contain as high as ~60–70wt% Fe_2O_3(t) and 16–20wt% TiO_2; the magnetite gabbros contain 18–55wt% Fe_2O_3(t) and 4–14wt % TiO_2 (Table S1). This is consistent with decrease of Fe-Ti oxides upward in these cyclic units. Although the Cr contents of both whole-rock and magnetite of the massive oxide layer at the base of cyclic unit II increase upward, they decrease upward in the other cyclic units (Figure 6a). Similar compositional reversals also occur in the Lower Zone at Damakan and Nalaqing, although there are less cyclic units at these locations than at Zhujiabaoabao (Figure 6b and 6c). Such synchronous variation between the Cr contents of whole-rock and magnetite also occurs in the magnetite layers in the Upper Zone of the Bushveld Complex [*Cawthorn and McCarthy*, 1980]. In each cyclic unit, forsterite (Fo) percentages of olivine always decrease upward. For instance, Fo of olivine vary from ~80 in the massive oxide to ~70 in the magnetite gabbros of the cyclic unit II and from ~81 in the massive oxide to ~65 in the gabbro of the cyclic unit V, respectively (Table S2b and Figure 6).

[21] For the Middle Zone at Zhujiabaobao, the magnetite gabbros at the bases of the cyclic units VI to XI have higher Fe_2O_3(t) and TiO_2 contents (20–40wt% and 7.5–13wt%, respectively) and lower SiO_2 and Al_2O_3 contents (30–36wt% and 8–12wt%, respectively, except for two samples) than the gabbros at the tops (Table S1 and Figure 6a). From the base to the top of these cyclic units, whole-rock Fe^{3+}/Ti^{4+} ratios gradually decrease, with exception of cyclic unit XI. For the lower two cyclic units, Cr contents of magnetite and their host rocks decrease regularly upward (except for the cyclic unit VIII and X) (Figure 6a). Fosterite percentages of olivine crystals in the magnetite gabbro at the bases of the cyclic units range from 63 to 77, similar to those of the Lower Zone magnetite gabbros (Table S2 and Figure 6a). Olivine in the gabbros is very rare. From the base to the top of the Middle Zone at Nalaqing, contents of whole-rock Fe_2O_3(t) and Cr and Fe^{3+}/Ti^{4+} ratio decrease, whereas TiO_2 has a small variation (Figure 6c).

[22] The Upper Zone rocks at Zhujiabaobao and Nalaqing are notable in having extremely high P_2O_5 contents (1–3.5wt%) and high concentrations of REE and Y (Table S1). Although contents of Fe_2O_3 (t) and TiO_2 of the Upper Zone gabbros vary within relatively small ranges (13–21wt% and 3.5–6wt%, respectively), Fe^{3+}/Ti^{4+} increases upward at Zhujiabaobao, whereas $Al_2O_3/(K_2O + Na_2O)$ remains

[1] All Supporting Information may be found in the online version of this article.

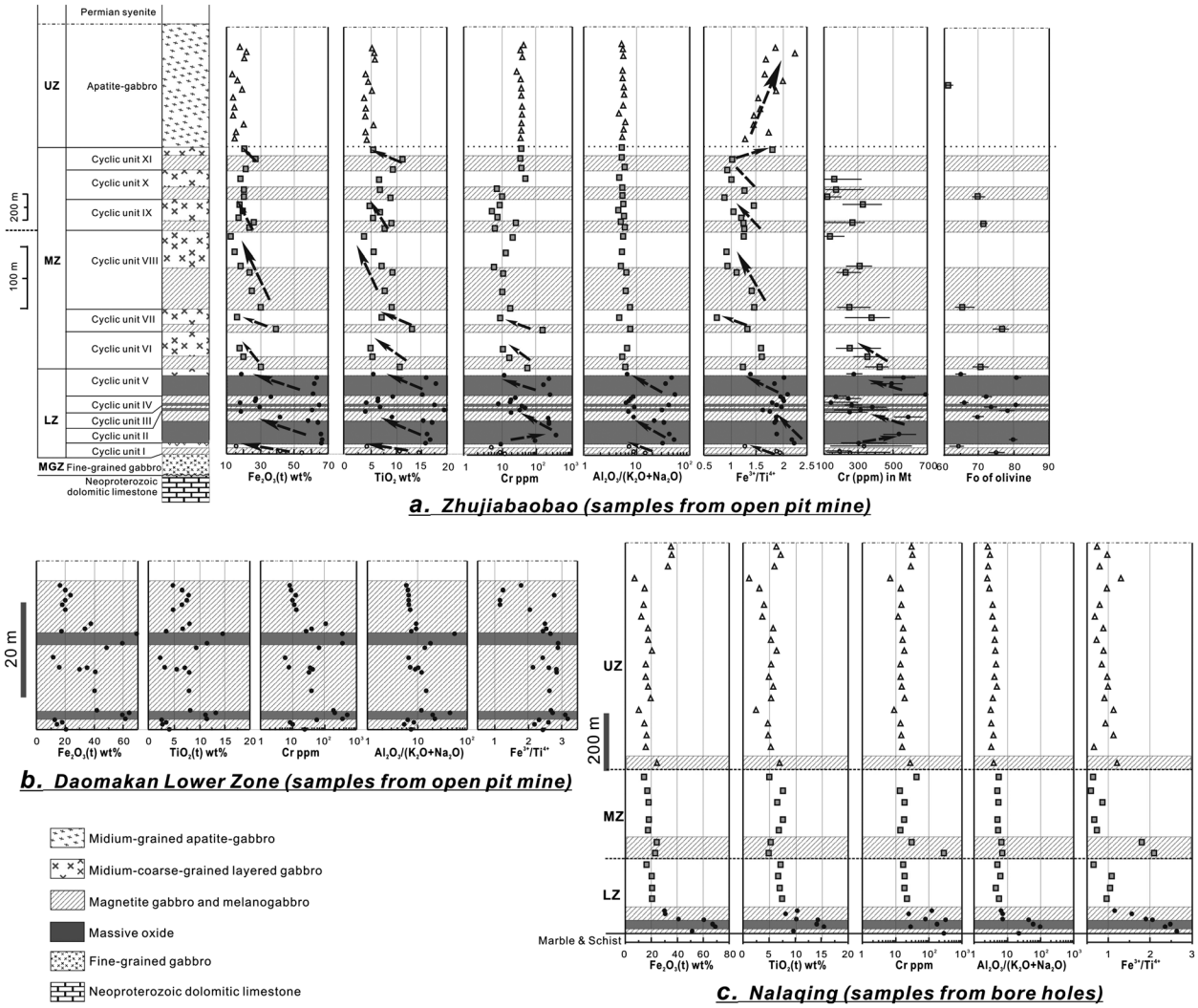

Figure 6. Chemostratigraphic columns of whole rock major oxides, ratios of $Al_2O_3/(K_2O+Na_2O)$ and Fe^{3+}/Ti^{4+}, and Cr contents of magnetite and forsterite percentages of olivine at (a) Zhujiabaobao (some data of olivine are from *Zhang et al*. [2011]), (b) Daomakan, and (c) Nalaqing.

constant (Figure 6a). Whole-rock contents of Fe_2O_3 (t), TiO_2 and Cr of the Upper Zone at Nalaqing display three cyclic variations (Figure 6c).

5.2. Chemical Correlations

[23] TiO_2 and V contents of the Panzhihua samples are well positively correlated with Fe_2O_3(t) (Figures 7a and 7c). The Middle Zone samples have TiO_2 contents higher than the Lower Zone samples at comparable Fe_2O_3(t) contents. TiO_2 contents of the Lower Zone samples at Zhujiabaobao and Nalaqing are higher than those at Daomakan (Figure 7a). For the samples of the Lower and Middle Zones, contents of P_2O_5 increase as Fe_2O_3(t) decreases. The Upper Zone apatite gabbros have the highest P_2O_5 contents (up to 3.2 wt%) and show a positive correlation with Fe_2O_3(t), implying a distinctive formation process. Although Cr contents of the Panzhihua samples are roughly positively correlated with Fe_2O_3(t), the massive oxides and magnetite gabbros at Zhujiabaobao have large variation in Cr contents (~10 ppm–500 ppm) (Table S1 and Figure 7d). The Lower Zone samples display a positive correlation between TiO_2 and Ga, whereas the Upper Zone samples show negative correlations (Figure 7e). In contrast, Nb contents of the samples of the Middle and Upper Zones increase with the increasing of TiO_2, and those of the Lower Zone samples increase slightly (Figure 7f). Figure 7g shows a correlation between Fe_2O_3(t) content and $Al_2O_3/(K_2O+Na_2O)$ ratio; the massive oxides have the highest Fe_2O_3(t) contents and the highest $Al_2O_3/(K_2O+Na_2O)$ ratios.

[24] The Lower Zone massive oxides and magnetite gabbros at Daomakan have conspicuously higher

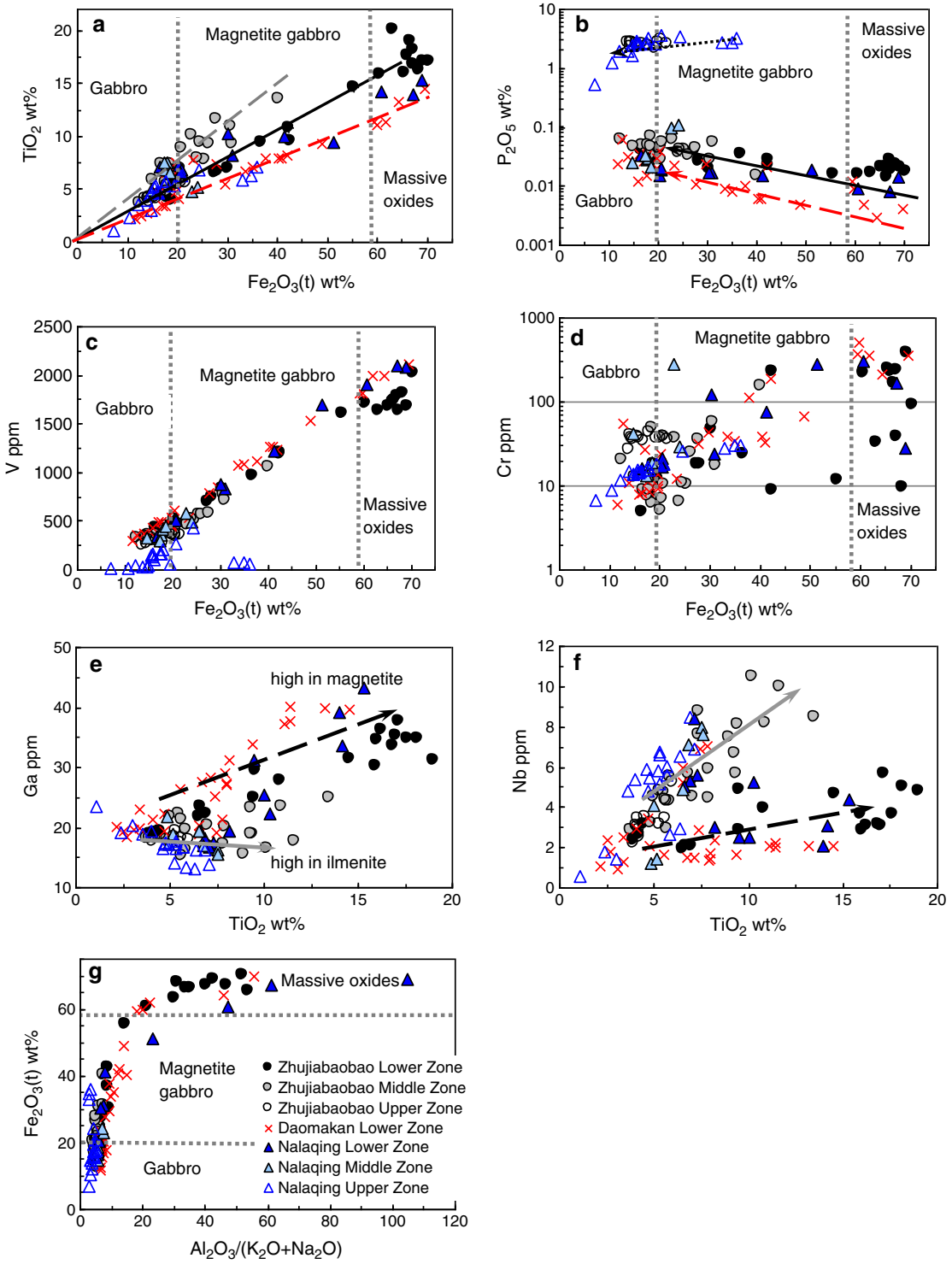

Figure 7. Whole rock binary plots. (a) TiO_2 versus $Fe_2O_3(t)$, (b) P_2O_5 versus $Fe_2O_3(t)$, (c) V versus $Fe_2O_3(t)$, (d) Cr vs $Fe_2O_3(t)$, (e) Ga versus TiO_2, (F) Nb vs SiO_2, and (g) $Fe_2O_3(t)$ versus $Al_2O_3/(K_2O + Na_2O)$.

Fe^{3+}/Ti^{4+} ratios than those at Zhujiabaobao and Nalaqing at the comparable contents of $Fe_2O_3(t)$, and the gabbros have a large variation in Fe^{3+}/Ti^{4+} ratio (Figure 8a). The Fe^{3+}/Ti^{4+} ratios of the Lower Zone samples are higher than those of the Middle Zone samples at both Zhujiabaobao and Nalqing, except for a few samples. The massive oxides at Zhujiabaobao have higher TiO_2 contents than those at Daomakan and Nalaqing at comparable Fe^{3+}/Ti^{4+} ratios (Figure 8b). Figure 8c shows a positive

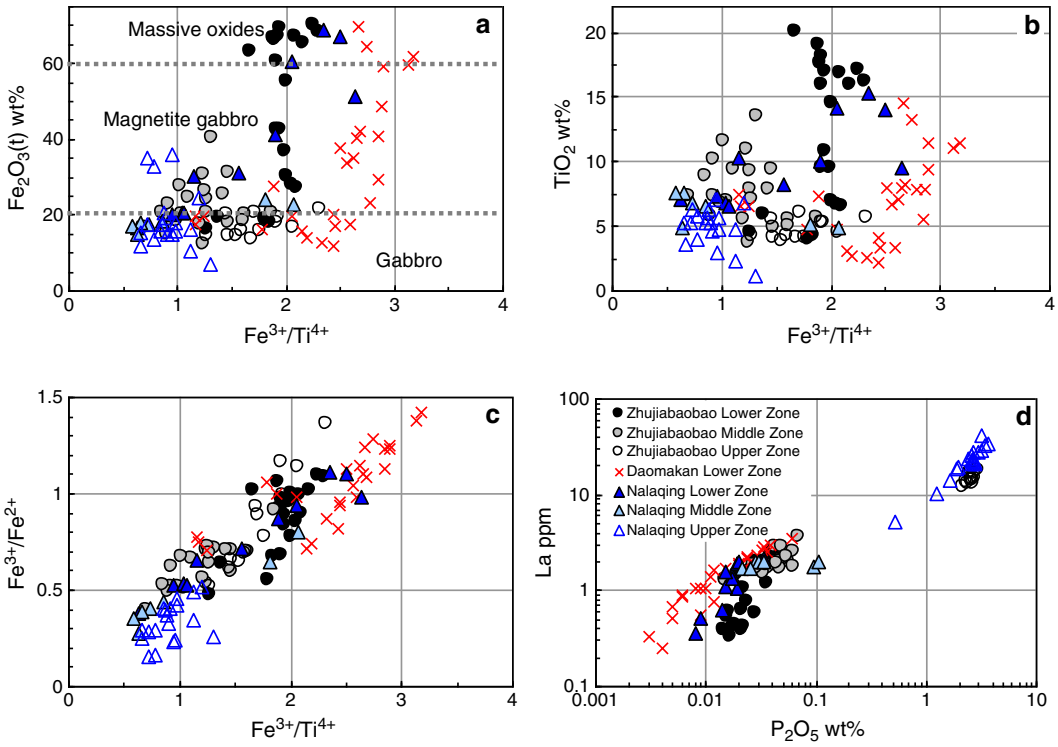

Figure 8. Binary plots of whole rock (a) $Fe_2O_3(t)$, (b) TiO_2, and (c) Fe^{3+}/Fe^{2+} against Fe^{3+}/Ti^{4+} and (d) La versus P_2O_5.

correlation between ratios of Fe^{3+}/Fe^{2+} and Fe^{3+}/Ti^{4+}. The positive correlation between La and P_2O_5 indicate that apatite is the main phase containing rare earth elements because of their high apatite/silicate melt partition coefficients (Figure 8d) [*Ionov et al.*, 1997].

5.3. Trace Elements and Sr-Nd Isotopes

[25] As shown in primitive mantle normalized trace element diagram, the massive oxides of the Lower Zone are characterized by extremely high positive anomalies of Ti and Nb and Ta (Figure 9a). The massive oxides at Daomakan and Nalaqing are distinct from those at Zhujiabaobao by evidently negative P anomalies and positive Sr anomalies (Figure 9a). Although the magnetite gabbros of both Lower and Middle zones have similar trace element compositions, those of the Lower Zone show less positive Nb and Ta anomalies and more extensively negative P anomalies (Figure 9b and 9c). The apatite gabbros of the Upper Zone are distinguishable from the gabbros of the Lower and Middle zones by highly enrichment of P and REE and strong depletions of Zr and Hf (Figures 9f).

[26] The samples of the three zones of the Panzhihua intrusion have similar Sr-Nd isotope values and plot in the oceanic island basalt (OIB) field in the $\epsilon_{Nd(260Ma)}$ versus $(^{87}Sr/^{86}Sr)_{260Ma}$ plot (Table S3 and Figure 10) [*Wilson*, 1989] and have much narrower ranges of $\epsilon_{Nd(260Ma)}$ (1.64–2.85) and $(^{87}Sr/^{86}Sr)_{260Ma}$ (0.7043–0.7046) than the high-Ti Emeishan basalts, which are considered to have experienced weaker crustal contamination than the low-Ti Emeishan basalts [*Xu et al.*, 2001; *Xiao et al.*, 2004; *Qi and Zhou*, 2008; *Zhou et al.*, 2008; *Song et al.*, 2008b, 2009].

6. Discussion

[27] Since Fe-Ti oxides commonly crystallize in later stage of fractionation of tholeiitic magmas, Fe-Ti oxide accumulation generally occurs in the upper parts of layered intrusions. For the Skaergaard intrusion, iron enrichment has been suggested to continue well past the appearance of Fe-Ti oxides [*Wager and Brown*, 1967; *McBirney and Hunter*, 1995; *Morse*, 1990; *McBirney*, 1989]. *Hunter and Sparks* [1987, 1990] argued that the Skaregaard magma is characterized by Fe and Ti depletion and silica enrichments from the start of the LZc with the onset of Fe-Ti oxides fractionation. The experimental performed by *Toplis and Carroll* [1996] further indicated that iron enrichment due to crystallization of olivine, plagioclase and clinopyroxene are restricted by the crystallization of Fe-Ti oxide minerals. Crystallization

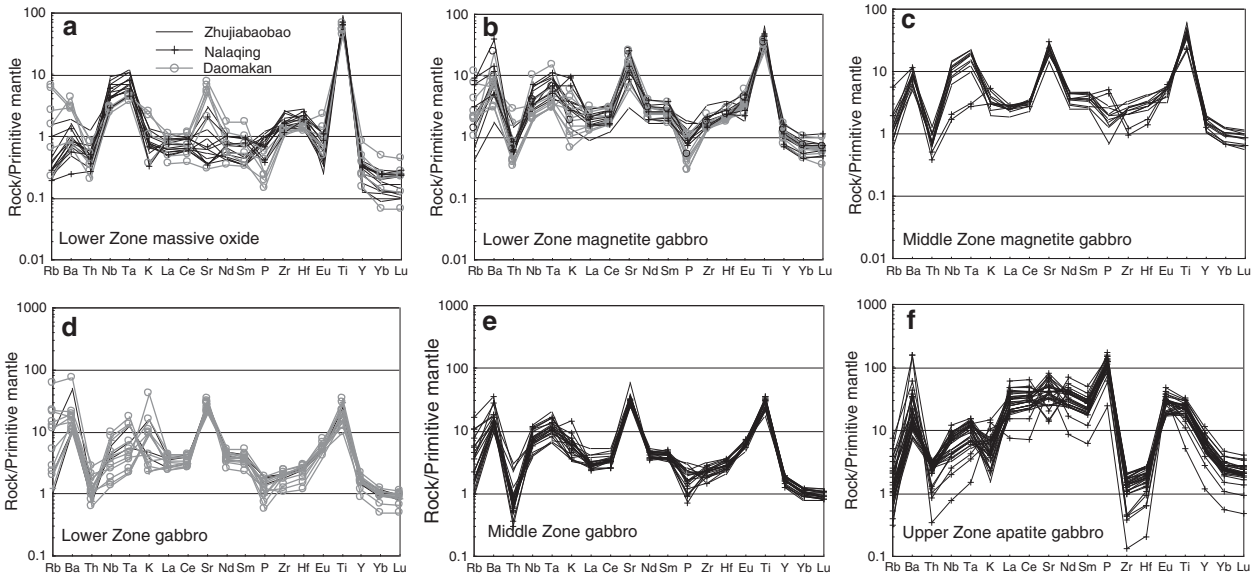

Figure 9. Primitive mantle normalized trace element diagrams. Trace element concentrations of the primitive mantle are from *Sun and McDonough* [1989].

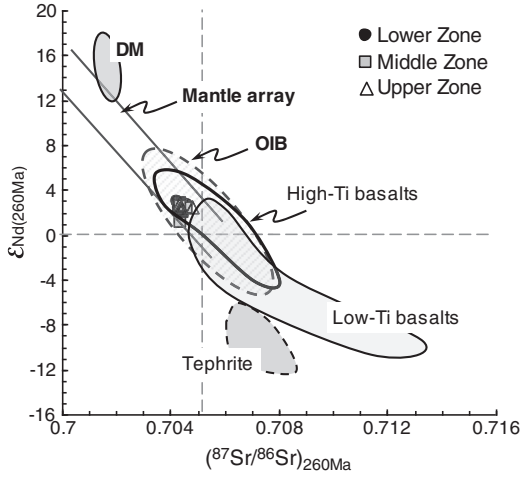

Figure 10. Diagram of $\epsilon_{Nd(260Ma)}$ versus $(^{87}Sr/^{86}Sr)_{260Ma}$, showing the genetic links between the Panzhihua gabbro and the high-Ti Emeishan flood basalts [*Xiao et al*., 2004; *Song et al*., 2008b].

of Fe-Ti oxides leads to stronger iron depletion and silica enrichment in system open to oxygen than in system closed to oxygen with decreasing temperature. This difference is due to that the dominant crystallized Fe-Ti oxide phase is magnetite in open system processes, and the importance of ilmenite increased in closed system processes. The thick Fe-Ti oxide-rich troctolite in the Layered Series comprising the low portion of the Sept Iles layered intrusion was attributed for the early crystallization of Fe-Ti oxides together with olivine and plagioclase from a ferrobasaltic parent magma [*Namur et al*., 2010]. Thus, the appearance of the thick massive Fe-Ti oxide layer at the base of the cyclic units of the Lower Zone indicates that the parental magmas had become Fe-Ti-enriched before entering the intrusion, and thus reached magnetite saturation early in the Panzhihua intrusion.

[28] Experimental studies have indicated that elevation of $Na_2O + K_2O + P_2O_5 + TiO_2$ in low pressure promotes the development of two immiscible liquids [*Charlier and Grove*, 2012]. The more Fe-rich immiscible liquid is not only high in Fe_2O_3 and TiO_2, but also high in P_2O_5, MgO, CaO, Zr, and REE, whereas the more silica-rich liquid has greater K_2O, Na_2O, Al_2O_3, and Rb contents [*Philpotts*, 1982; *Philpotts and Doyle*, 1983; *Naslund*, 1983; *Veksler et al*., 2006]. *Reynolds* [1985] and *Van Tongeren and Mathez* [2012] argued that the nelsonite layers containing ~70% Fe-Ti-oxides and ~30% apatite in the Upper Zone of the Bushveld Complex were associated with liquid immiscible. *Song et al*. [1994] proposed that the Panzhihua massive oxide layers were produced by immiscible Fe-Ti oxide liquids. *Zhou et al*. [2005] further suggested that this oxide liquid was separated from a Fe-Ti-rich mafic magma, which in turn immiscibly separated from strongly fractionated mafic magmas. An Fe-rich liquid would be high in density and low in viscosity and thus would be able to percolate through silicate crystal mushes [*Cawthorn and Ashwal*, 2009]. However, such phenomenon had not been observed in the Panzhihua intrusion. The massive oxide layers grade upward to magnetite gabbros and then gabbros in the cyclic units of the

Panzhihua intrusion (Figure 6). Particularly, study of Fe-Ti oxide inclusions in olivine crystals of the Panzhihua and Hongge intrusions indicated that these oxides were primocrysts and crystallized together with olivine from a common magma, rather than immiscible Fe-Ti rich liquid [*Pang et al*., 2008a, 2008b]. Thus, the stratiform massive Fe-Ti oxide ore layers in the Panzhihua intrusion were most likely produced by sinking and sorting of dense Fe-Ti oxide crystals. However, why and how the thick massive Fe-Ti oxide layers were formed and how the magma became Fe-Ti-enriched before it entered the Panzhihua magma chamber and direction of the magma flowing, remain poorly understood and unexplained.

[29] Petrographic features of layered intrusions are not only related to solidification processes (e.g., fractional crystallization and compositional diffusion), but are also linked to fluid dynamic processes (e.g., magma replenishment and convection, mixing of the replenished magma) and thermodynamic conditions (e.g., temperature, pressure, f_{O2} and compositions of the magma). Therefore, this study focuses on the significance of the coupling between magma replenishment and fractionation, and the role of variations in physical property of the magma during crystallization on the formation of the thick Fe-Ti oxide layers in the Panzhihua intrusion.

6.1. Multiple Magma Replenishment

[30] A simple mass balance calculation indicates that if crystallization of Fe-Ti oxides resulted in ~3 wt% Fe_2O_3(t) removal, and the formation of the 60 m and 40 m thick massive ore layers at the base of the cyclic units II and V requires ~2000 m and ~1500 m thick magma layers, respectively. It is difficult to imagine that such huge massive magma volume could be input by a single pulse of magma, because the Panzhihuan intrusion is only about 2000 m thick, although top of the intrusion have been cut off by a fault (Figure 3). This means that repeating replenishment of magma occurred during the formation of the massive oxide layers. The repeating replenishment of relatively primary magma and fractional crystallization are also indicated by the periodically reversals of Cr contents of magnetite in the cyclic units of the Lower Zone (Figure 6a). These phenomena suggest that the Panzhihua intrusion was a chamber in a magma plumbing system, in which the composition of the magma at the base of the magma chamber is periodically modified due to repeated recharge of more primary magma.

[31] The Fo contents of olivine crystals in the Panzhihua rocks are <81 (Table S2 and Figure 6a), significantly lower than those in equilibrium with the primary mantle-derived mafic magma (Fo = 88–90). Thus, the magmas must have experienced extended fractional crystallization before they entered the Panzhihua intrusion. High Pd/Ir values (14–24) in Panzhihua, much higher than that of the primitive mantle (~1.2) [*Sun and McDonough*, 1989], are also a signature of highly fractionated magmas [*Zhou et al*., 2005]. The magnetite exsolution lamellae in the clinopyroxene crystals of the Lower and Middle Zones demonstrate that the fractionated parental magmas were Fe-Ti-enriched (Figure 5c). A most likely mechanism is that these Fe-Ti-enriched parental magmas were formed through fractionation of a more primitive magma in a deep-seated magma chamber.

[32] A genetic link between the Panzhihua intrusion and the Permian high-Ti Emeishan flood basalts is indicated not only by the zircon SHRIMP U-Pb age of 263 ± 3 Ma of the Panzhihua intrusion [*Zhou et al*., 2005] but also by their similar Sr-Nd isotope compositions (Figure 10). Relatively constant $\epsilon_{Nd(260Ma)}$ (=1–3) and $(^{87}Sr/^{86}Sr)_{260Ma}$ (=0.7043–0.7048) suggest a weak crustal contamination and fractionation control magma evolution. Published data indicate that the Fe_2O_3(t) and TiO_2 contents of the high-Ti Emeishan flood basalts increase up to ~18wt% and ~5wt%, respectively, as MgO decreases to ~6wt%, and then they both decrease quickly, probably associated with Fe-Ti oxide crystallization and removal as MgO decreases further [*Song et al*., 2001; *Xiao et al*., 2004]. Such compositional variation is consistent with a Fenner trend, which results in tholeiitic magmas evolving to more Fe-enriched before Fe-Ti oxide crystallization [*Brooks et al*., 1991].

[33] Key questions are whether and how fractionation in a deep-seated magma chamber can produce Fe-Ti enriched mafic magmas, and whether or not Fe-Ti oxides can crystallize early in the shallower magma chamber.

6.2. Crystallization at Different Depths—Insights from MELTS Calculations

[34] It is difficult to estimate the composition of a parental magma of layered intrusion based on marginal zone rocks, as the latter may have been produced by extensive interaction of magmas with wall-rocks. However, melt inclusions hosted by olivine phenocrysts with high Fo percentage in the picritic lava are helpful to estimate the parental magma composition of the related intrusions.

We assume that the primary magma of the Panzhihua intrusion had a composition similar to the melt inclusion (M3 24) hosted in high Fo olivine phenocryst (Fo = 89.1) of the Emeishan high-Ti picrite [*Kamenetsky et al*., 2012]. The melt inclusion contains 12.12wt% FeO, 13.94wt% MgO, and 2.94wt % TiO_2. The slightly lower Fo of the olivine phenocryst than that of olivine of the Phanerozoic mantle [*Gaul et al*., 2000] is probably because of existence of garnet pyroxenite in the mantle source [*Kamenetsky et al*., 2012]. We use the MELTS package [*Ghiorso and Sack*, 1995] modified by *Asimow and Ghiorso* [1998] to model the hidden fractionation in the deep-seated magma chamber and then that in the Panzhihua chamber under oxygen fugacity (f_{O2}) of FMQ (quartz-fayalite-magnetite buffer). Results are listed in Tables S4 and S5. Although the Panzhihua intrusion was emplaced in a Neoproterozoic dolomite and sandstone [*Ganino et al*., 2008], the Hongge and Xinjie layered intrusions are in contact with Emeishan flood basalts [*Panxi Geological Unit*, 1984], implying that these layered intrusions formed at shallow depth. Thus, we assume that the Panzhihua intrusion crystallized at ~1 kbar, and we take the pressure of the deep-seated magma chamber to be 5 kbar, which is roughly consistent with crystallization pressure of the clinopyroxene phenocrysts in the Emeishan basalts (Y. Tao, personal communication).

[35] MELTS calculations indicate that at 5 kbar, spinel is the liquidus phase (1397°C) if the primary magma has composition of the melt inclusion, followed by olivine and clinopyroxene appearance at 1348 and 1321°C, respectively (Table S4). The spinel is high in Cr_2O_3 (45.3–13.2wt%) and olivine has high Fo (87–86) (Table S4), which are roughly consistent with the compositions of these minerals of the high-Ti picrite [*Kamenetsky et al*., 2012]. After fractional crystallization of 0.77wt% spinel, 2.4wt% olivine and 42.8wt% clinopyroxene, the Fe_2O_3(t) and TiO_2 contents in the magma increase to ~16.5wt% and 4.9wt%, respectively (Tables S4 and S5). We assume that such Fe-Ti-enriched magma is the parental magma of the Panzhihua intrusion.

[36] In the shallower magma chamber at ~1 kbar, olivine crystallized from the Fe-Ti enriched magma at 1190°C followed by plagioclase when temperature decreases to 1161°C (Table S4). Magnetite crystallizes when magma Fe_2O_3(t) and TiO_2 increase to 19.1wt% and 5.4wt% at ~1151°C after fractional crystallization of ~4.4% olivine and ~5.6% plagioclase (Tables S4 and S5). This indicates that magnetite is an early crystallized phase in the shallow magma chamber. As the temperature decreases from 1190°C to 1130°C, the An (anorthite percentage) of crystallized plagioclase decreases from 69 to 56, Fo of olivine decreases from 80 to 72 (Table S4). This is consistent with the electron microprobe data of plagioclase (An = 49–72, Pang et al., 2009) and olivine (Fo = 61–81, Table S2) of the Panzhihua gabbros. Magnetite exsolution resulted in Mg values of the clinopyroxene (70–80) measured by electron microprobe [*Pang et al*., 2009] higher than the MELTS calculation (64–75, Table S4). After fractional crystallization of 11.2% magnetite, the contents of Fe_2O_3(t) and TiO_2 of the residual magma decrease quickly to 15.7wt% and 3.7wt%, respectively, at 1130°C (Tables S4 and S5). Ilmenite is commonly subhedral and interstitial in the massive oxides and magnetite gabbros and is expected to be crystallized later than magnetite and silicate minerals. Thus Fe^{3+}/Ti^{4+} ratios decrease upward in each cyclic unit in the Lower and Middle Zones (Table S4 and Figure 6). The MELTS calculations are broadly consistent with the compositional variations of the high-Ti Emeishan basalts, where Fe_2O_3(t) and TiO_2 contents reach maximum values when MgO contents lie from 5 to 6wt% (Figure 12) [*Xu et al*., 2001; *Xiao et al*., 2004; *Song et al*., 2008b, 2009].

[37] Although MELTS calculation predicts ilmenite crystallizing later than apatite, ilmenite must crystallize earlier than apatite in fact, because ilmenite is one of the major cumulus phases in the massive oxides and magnetite gabbros of Lower and Middle Zones. MELTS calculation predicts MgO contents of magnetite (10–12wt%) higher than electron microprobe measurement (2–3wt%) (Tables S2 and S4), probably is because that few experimental data for ferrobasaltic systems have been used in the construction of the MELTS model [*Toplis and Carroll*, 1996]. In the shallow magma chamber at ~1 kbar, the liquidus temperature (1190°C) is as much as 50°C lower than the temperature of the Fe-Ti enriched magma raised from deep level (1240°C) (Table S4). This implies that the new hot magma is able to melt the crystallized minerals although the temperature must decrease during the magma rising. Thus, minerals crystallized from the mixed magma will have more complicated compositions than those predicted by MELTS (see above). Another possible reason is that the assumptions about parental and evolved magmas are too conservative.

6.3. Formation of Thick Fe-Ti Oxide Layers—Fluid Dynamical Consideration

[38] The olivine crystals hosting magnetite inclusions high in Cr_2O_3 (up to 2.2wt%) are high in Ni

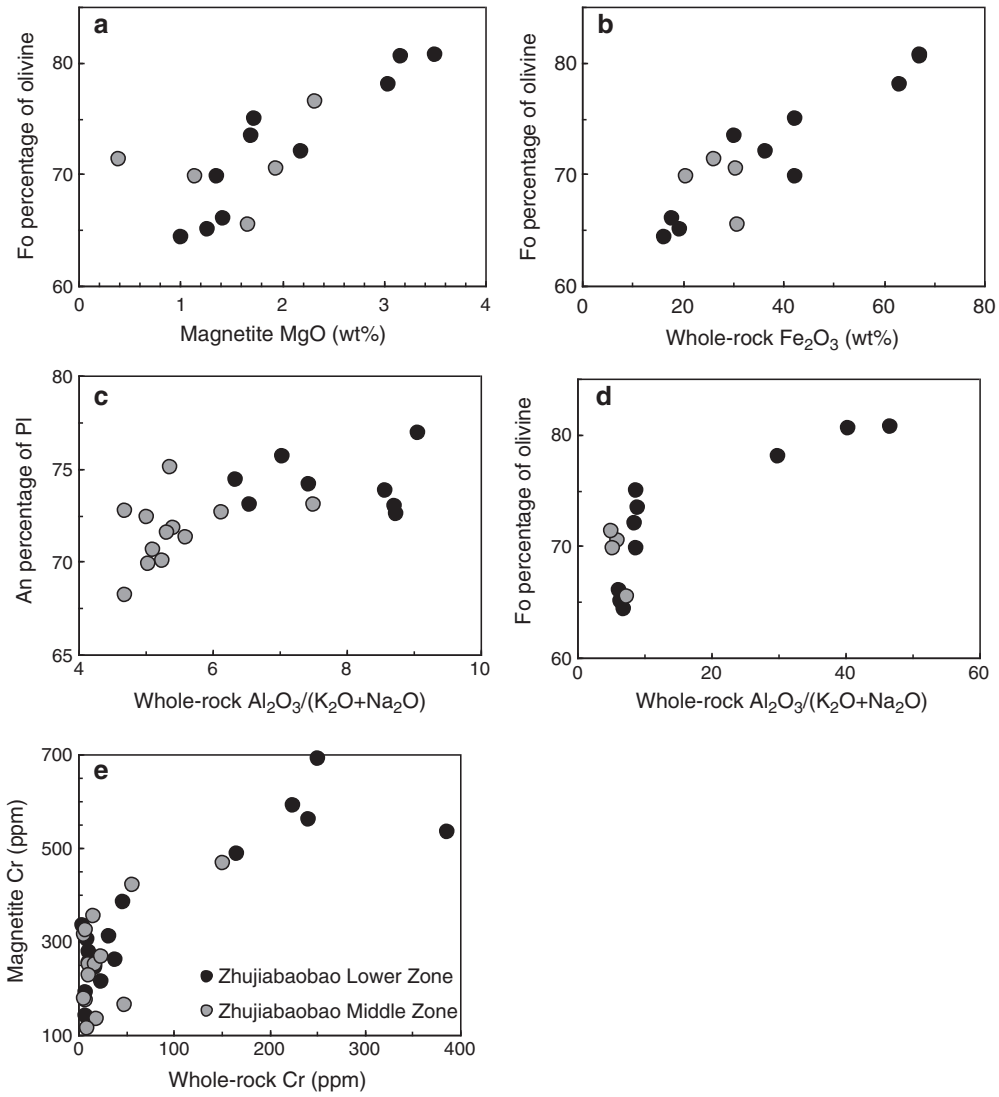

Figure 11. Plot of forsterite percentage of olivine against (a) MgO content of magnetite and (b) whole-rock Fe_2O_3 contents, (c) anorthite percentage of plagioclase, and (d) forsterite percentage of olivine against whole-rock $Al_2O_3/(K_2O+Na_2O)$ ratio. (e) Cr content of magneite versus whole-rock Cr content.

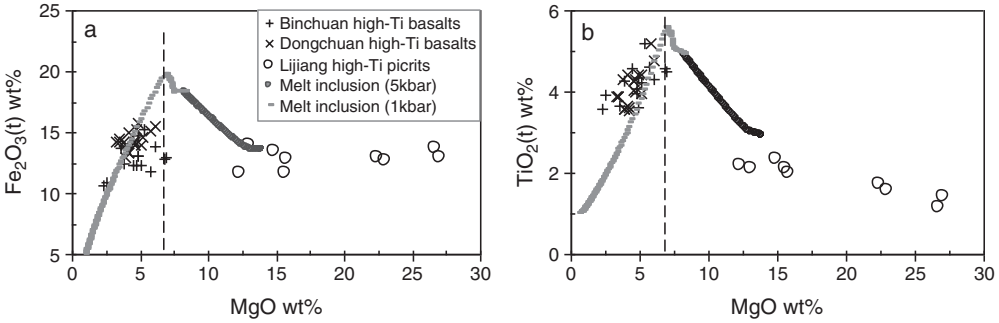

Figure 12. Results of the MELTS calculations of fractional crystallization at two depths and the compositions of the high-Ti Emeishan flood basalts [*Xiao et al.*, 2004; *Song et al.*, 2008b].

(800–2400ppm), which only occur rarely in olivine melagabbro [*Pang et al.*, 2008b, 2009]. Most olivine in the Panzhihua intrusion has Ni contents <250 ppm (Table S2). This implies that there are two generations of olivine; early generation olivine from the depth has higher Fo and Ni contents than

the later generation olivine crystallized in the Panzhihua intrusion.

[39] As mentioned above, experimental studies have indicated that Fe-Ti oxides commonly crystallize in later stage of fractionation of tholeiitic magmas [*Toplis and Carroll*, 1996; *Thy et al*., 2006]. Early saturation of Fe-Ti oxides in the magma can be resulted from enriched in Fe-Ti or high f_{O2} [*Namur et al*., 2010]. Magnetite exsolution lamellae in the clinopyroxene of the rocks of the Panzhihua Lower and Middle Zones (Figure 5c) indicate that the parental magmas were enriched in Fe-Ti. Above MELTS calculation suggest that such Fe-Ti-enriched magma can be produced by fractionation of picritic magma at depth (Table S4). The dominant factors controlling formation of a thick, stratiform Fe-Ti oxide layers (particularly the massive oxide layers) at the base of a magma chamber include (1) early crystallization of Fe-Ti oxides, (2) injection and emplacement of evolved Fe-Ti-enriched magmas along the base of the magma chamber, and (3) frequent replenishment of the Fe-Ti-enriched magmas.

[40] That magnetite is one of the early crystallizing phases together with olivine and plagioclase at 1 kbar (Table S4) is supported by the positive correlations between Fo percentage of olivine and MgO content of magnetite as well as whole-rock Fe_2O_3 content (Figures 11a and 11b) and the positive correlation between whole-rock Fe_2O_3(t) and $Al_2O_3/(K_2O+Na_2O)$ (Figure 7f). Plagioclase is the most important mineral containing Al_2O_3, Na_2O and K_2O in the Panzhihua intrusion, and thus whole-rock $Al_2O_3/(K_2O+Na_2O)$ ratios are positively correlated with An contents of plagioclase. The densities of the magmas increase from 2.85 to 2.91 g/cm^3 after fractional crystallization of 0.77wt% spinel, 2.4wt% olivine, and 42.7wt% clinopyroxene in the deep-seated magma chamber (Table S4). This density is lower than that of the magnetite (4.3–4.8 g/cm^3) and olivine (3.3–3.8 g/cm^3), but larger than that of plagioclase (2.63–2.65 g/cm^3) (Table S4). In the shallower magma chamber, therefore, even if the magnetite crystallizes slightly later than olivine and plagioclase, it still can be winnowed out from the plagioclase-olivine-magnetite-magma mixture and settled to the floor during the slurry flowing along the base of the magma chamber. Whereas, plagioclase will float in the magma because of its low density, then the massive oxides only contain very minor plagioclase. This mechanism also played an important role for the formation of the Upper Border anorthosite of the Sept Iles layered intrusion [*Namur et al*., 2011].

[41] In the shallow magma chamber, the density of the magma decreases to 2.74 g/cm^3 after crystallization of olivine, plagioclase, magnetite and clinopyroxene, lower than that of the Fe-Ti enriched magma replenished from the deep-seated magma chamber (2.91) (Table S4). Thus, when a new pulse of the Fe-Ti-enriched magma intruded into the Panzhihua intrusion, it would have formed a laminar flow along the base of the magma chamber [*Campbell and Turner*, 1989; *Snyder and Tait*, 1995], although it is difficult to estimate the height of rise of the magma fountain because the width of the feeder dyke is unknown. The widespread planar foliation and lineation shown by the orientation of plagioclase and clinopyroxene in the rhythmic layering defined by modal variation of magnetite and clinopyroxen and plaioclase (Figures 5b and 5d) indicates the magmatic currents resulted from replenishment of magma [*Wager and Brown*, 1967; *Irvine*, 1987; *Conrad and Naslund*, 1989]. Compaction or subsolidus growth of the minerals probably also played roles for the mineral foliation [*McBimey and Hunter*, 1995; *Fyfe*, 1976].

[42] Chromium is strongly compatible to magnetite and ilmenite [*Schock*, 1979; *Duchesne et al*., 1985; Table S6]. Normal (decreasing Cr content) and reverse (increasing Cr content) trends alternate of magnetite and their whole-rocks in the cyclic units II to V imply crucial contribution of frequently emplacement of more primitive magma on the formation of the cyclic units and the thick massive oxide layers. This is similar to the formation of the Allard Lake ilmenite deposit in Canada [*Charlier et al*., 2010]. Because apatite is rare in the Lower and Middle Zones and the magnetite crystallized extensively, we assume that emplacement of new more primitive magma always occurred before apatite began to crystallize for the two zones (Table S4). If the proportion between the Fe-Ti-enriched magma (1240°C) from the deep level and the resident magma (1130°C) in the shallower magma chamber is more than 7:3 and if the compositions assumed for the two magmas are correct, the mixed magma would contain >17.6wt% Fe_2O_3(t) and >4.5wt% TiO_2 and magnetite will remain an early crystallizing phase. Thus, the thick Fe-Ti oxide-rich cumulates can be produced by Fe-Ti oxide crystallization from the fractionated Fe-Ti enriched magma frequently recharged from a deep-seated magma chamber. Continuous emplacement of ferrobasaltic magma and early crystallization and accumulation of ilmenite also played important role in the formation of the world class Allard Lake ilmenite deposit in the Havre-Saint-Pierre anorthosite

complex, Canada [*Charlier et al*. 2010]. Magma emplacements and magma mixing have been indicated by normal and reverse fractionation trends of Cr content in cumulus ilmenite.

[43] Although previous studies suggested that Nb and Zr are incompatible for magnetite [*Paster et al*., 1974; *Schock*, 1979], recent experimental data have indicated that the partitioning behaviors of these elements are controlled by the major element composition of the magnetite [*Nielsen et al*., 1994, *Nielsen and Beard*, 2000]. The partition coefficients for these elements between magnetite and mafic to intermediate magmas may be larger than 1 and are positively correlated with Ti content of the magnetite and negatively correlated with Al and Mg contents. The magnetites of the massive oxides are very high in TiO_2 (12–19 wt%, Table S2), and therefore, it is expectable that these elements are moderately enriched in the magnetite. Moreover, Nb and Ta are compatible to ilmenite [*Ionov et al*., 1997, Table S6]. Thus, the remarkable enrichments of Nb, Ta, Zr, and Hf relative to other trace elements in the massive oxides (Figure 9a) indicate that these elements are compatible to Fe-Ti oxides in the Panzhihua intrusion.

6.4. Lateral Variation of Fe-Ti Oxide Layer Thickness

[44] The compositions of the massive oxides and magnetite gabbros and their lithostratigraphic variations depend on the crystallization order of the magnetite and ilmenite and the proportion between them. Oxygen fugacity is found to have a large influence on the stability of Fe-Ti oxides [*Snyder et al*., 1993]. Experiments have shown that magnetite appears earlier than ilmenite above the FMQ buffer in basaltic magma and the order may reverse below FMQ [*Snyder et al*., 1993; *Toplis and Carroll*, 1995]. Thus, decreases of the Fe^{3+}/Ti^{4+} ratios from the base to the top of most cyclic units of the Lower and Middle Zones suggest a slightly decreases of f_{O2} during the formation of each cyclic unit because of a large amount of magnetite (Table S5 and Figure 6).

[45] The different trends displayed in the diagrams of TiO_2 against Fe_2O_3(t) suggest that the Lower and Middle Zones were produced by different processes. The massive oxides and gabbros of the Lower Zone have higher Fe_2O_3(t)/TiO_2 than those of the Middle Zone (Figure 7a), indicating that the Lower Zone has relatively higher magnetite/(magnetite + ilmenite) ratio and crystallized at a relatively higher f_{O2} than the Middle Zone. Accordingly, the Lower Zone rocks have higher Fe^{3+}/Ti^{4+} and Fe^{3+}/Fe^{2+} values than the Middle Zone rocks at the same TiO_2 and Fe_2O_3(t) contents (Figure 8).

[46] On the other hand, the ratios of Fe_2O_3(t)/TiO_2, Fe^{3+}/Ti^{4+} and Fe^{3+}/Fe^{2+} of the Daomakan Lower Zone rocks are visibly higher than those at Zhujiabaobao and Nalaqing (Figures 7a and 8), suggesting that the Lower Zone at Daomakan formed under high f_{O2} relative to that at Zhujiaobaobao and Nalaqing. Chromium is strongly compatible to magnetite and $D_{Cr}^{magnetite/magma}$ is as high as 153 [*Schock*, 1979, Table S6]. Thus, the higher Cr contents of the massive oxides at Daomakan than those at Zhujiabaobao and Nalaqing imply that the magnetite crystallized relatively earlier at Daomakan (Table S1 and Figures 6 and 7e). Partition coefficients of V and Ga between magnetite and basaltic magma ($D_V^{magnetite/magma} = 26$, $D_{Ga}^{magnetite/magma} = 2$) are higher than $D_V^{ilmenitea/magma}$ (=9) and $D_{Ga}^{ilmenite/magma}$ (=0.14), whereas, $D_{Nb}^{magnetite/magma}$ (=0.4 or >1) is lower than $D_{Nb}^{ilmenite/magma}$ (=2.3) [*Paster et al*., 1974; *Schock*, 1979; *Villemant et al*., 1981; *Duchesne et al*., 1985; *Nielson et al*., 1994, 2000]. Thus, the decreases of V and Ga and increase of Nb of the Lower Zone samples from Damakan to Zhujiabaobao and Nalaqing at comparable Fe_2O_3 and TiO_2 contents also indicate a decreasing magnetite/(magnetite + ilmenite) ratio and f_{O2} during accumulation of the Fe-Ti oxides (Figures 7c, 7e, and 7f). The above phenomena indicate crystallization of magnetite early at Daomakan and imply that the Fe-Ti-enriched magmas from deep level entered the Panzhihua intrusion at Daomakan and flowed toward to Zhujiabaobao and Nalaqing. More magma slurry flowed to the more concave-down Zhujiabaobao, where more Fe-Ti oxides crystallized and settled down to form the extremely thick massive oxides and magnetite gabbros layers.

[47] The formation of the very thick stratiform massive Fe-Ti oxide layers at the bases of the cyclic units II and V and relatively constant contents of Fe_2O_3 (t), TiO_2, high V and Ga contents and high ratios of Fe_2O_3(t)/TiO_2 and Fe^{3+}/Ti^{4+} (Figures 6–8) requires accumulation of Fe-Ti oxides from continually replenished Fe-Ti-enriched magmas. Additionally, increases of Cr contents of the magnetites and their whole-rocks from the base of the massive oxide layer of the cyclic unit II upward probably indicate compositional variation of the recharged magmas from the deep level (Figure 6a). Whereas, low contents of V and Ga and Fe_2O_3(t)/TiO_2 ratios of the magnetite gabbros of the Middle Zone have implied that the magma replenishment was not frequent enough and mixing with residual magma (Figure 7).

6.5. Concentration of P and REE in the Upper Zone

[48] Phosphorus is incompatible in silicate minerals and Fe-Ti oxides [*Jones*, 1995; *Bindeman et al*., 1998] during fractionation of mafic magmas and is thus concentrated in the residual magma before crystallization of apatite. The P_2O_5 saturation content of the Panzhihua magma is about 1.35wt% according to the MELTS calculation, which is consistent with the P_2O_5 content (1.3 ± 0.3wt%) at apatite saturation in the Upper Zone of the Bushveld Complex [*Cawthorn and Walsh*, 1988]. Thus, the trapped liquid contents in the Lower and Middle Zones are 1–4% (except for a few samples). This means that more interstitial liquid rich in P and REE migrated upward due to compression and mixed with the differentiated magma and resulted in apatite saturation in the Upper Zone.

[49] Rare earth elements are strongly compatible in apatite, although many factors such as temperature, SiO_2 content, and alkalinity can significantly affect partition coefficients (Table S1) [*Watson and Green* 1981; *Fujimaki*, 1986]. The partition coefficients of Gd and Yb between apatite and basaltic magma are 1.7 and 0.93 [*Ionov et al*., 1997], whereas $D_{Gd}^{apatite/andesite}$ and $D_{Yb}^{apatite/andesite}$ are as high as 43.9 and 15.4, respectively (Table S6) [*Fujimaki*, 1986]. This means that Gd/Yb ratio of crystallized apatite would elevate during extensive fractional crystallization. Thus, the remarkable high REE concentrations and Gd/Yb (7–11) again indicate that the Upper Zone apatite gabbros were crystallized from highly differentiated magmas (Table S1 and Figures 6–9). The three cyclic compositional variations in the Upper Zone imply that new magma injection and magma mixing also occurred during the formation of the Upper Zone.

7. Conclusion

[50] The Panzhihua intrusion was one magma chamber on a magma plumbing system replenished by fractionated and Fe-Ti-enriched mafic magmas from a deep-seated magma chamber, and from which the most evolved magmas had been tapped. In the deep-seated magma chamber, extensive fractionation of olivine and clinopyroxene resulted in Fe-Ti enrichment and a significant increase in the density of the residual fractionated magma. As a result, the hot and dense Fe-Ti-enriched magmas from the deeper level spread along the floor when injected into the shallow Panzhihua intrusion and magnetite became one of the early crystallizing phases. The density of this magma decreased after crystallization of Fe-Ti oxides. The thick, stratiform massive Fe-Ti oxide layers at the bases of the cyclic units in the Panzhihua Lower Zone were produced by Fe-Ti oxide accumulation from these frequently replenished Fe-Ti-enriched magmas. As the frequency of replenishment of the Fe-Ti-enriched magmas decreased, magnetite gabbros were formed along the bases of the cyclic units of the Middle Zone. In contrast, the Upper Zone apatite gabbros were formed by more evolved incompatible elements enriched magmas.

Acknowledgments

[51] This study was funded by the National Basic Research Program of China (2012CB416804) and research grants from State Key Laboratory of Ore Deposit Geochemistry (SKLODG-ZY125-06), and NSFC (40730420 and 40973038) to Xie-Yan Song. We thank Jian-Xiang Guan, L.V. Danyushevsky, A.J. Crawford, Tony Naldrett, and Mei-Fu Zhou for their kind helps on our study. We are also grateful to two anonymous reviewers and Joel Baker and Olivier Namur, whose constructive comments are significant for improving the manuscript. Hu J. and Huang Y. are thanked for their efforts in trace element analysis.

References

Asimow, P. D. and M. S. Ghiorso (1998), Algorithmic modifications extending MELTS to calculate subsolidus phase relations, *Am. Mineral.*, *83*, 1127–1132.

Bateman, A. M. (1951), The formation of late magmatic oxide ores, *Econ. Geol.*, *46*, 404–426.

Bindeman, I. N., A. M. Davis, and M. J. M. Drake (1998), Ion microprobe study of plagioclase-basalt partition experiments at natural concentration levels of trace elements, *Geochim. Cosmochim. Acta*, *62*, 1175–1193.

Brooks, C. K., L. M. Larsen and T. F. D. Nielsen (1991), Importance of iron-rich tholeiitic magmas at divergent plate margins: A reappraisal, *Geology*, *19*, 269–272.

Campbell, I. H. and J. S. Turner (1989), Fountains in magma chambers, *J. Petrol.*, *30*, 885–923.

Cawthorn, R. G. and T. S. McCarthy (1980), Variation in Cr content of magnetite from the Upper Zone of the Bushveld Complex—Evidence for heterogeneity and convection currents in magma chambers, *Earth and Planetary Science Letters*, *46*, 335–343.

Cawthorn, R. G. and T. G. Molyneux (1986), Vanadiferous Magnetite Deposits of the Bushveld Complex, in *Mineral Deposits of Southern Africa 2*., edited by Anhaeusser, C.R. and S. Maske, pp. 1251–1266, Johannesburg, Geological Society of South Africa.

Cawthorn, R. G. and K. L. Walsh (1988), The use of phosphorus contents in yielding estimates of the proportion of trapped liquid in cumulates of the Upper Zone of the Bushveld Complex, *Mineralogical Magazine*, *52*, 81–89.

Cawthorn, R. G. and L. D. Ashwal (2009), Origin of anorthosite and magnetitite layers in the Bushveld Complex, constrained by major element compositions of plagioclase, *J. Petrol.*, *50* (9), 1607–1637.

Charlier, B., O. Namur, S. Malpas, C. de Marneffe, J.-C. Duchesne, J. V. Auwera and O. Bolle (2010), Origin of the giant Allard Lake ilmenite ore deposit (Canada) by fractional crystallization, multiple magma pulses and mixing, *Lithos*, *117*, 119–134.

Charlier, B. and T. L. Grove (2012), Experiments on liquid immiscibility along tholeiitic liquid lines of descent, *Contributions to Mineralogy and Petrology*, *164*, 27–44.

Chung, S. L. and B. M. Jahn (1995), Plume–lithosphere interaction in generation of the Emeishan flood basalts at the Permian–Triassic boundary, *Geology*, *23*, 889–892.

Conrad, M. E. and H. R. Naslund (1989), Modally-graded rhythmic layering in the Skaergaard intrusion. *J. Petrol.*, *30*, 251–69.

Duchesne, J. C., I. Roelandts, D. Demaiffe and D. Weis (1985), Petrogenesis of monzonoritic dykes in the Egersund-Ogna anorthosite (Rogaland, S.W. Norway): Trace elements and isotopic (St, Pb) constraints, *Contributions to Mineralogy and Petrology*, *90*, 214–225.

Eales, H. V. (2000), Implications of the chromium budget of the Western Limb of the Bushveld Complex, *South Africa Journal of Geology*, *103*, 141–150.

Fujimaki, H. (1986), Partition coefficients of Hf, Zr and REE between zircon, apatite, and liquid, *Contributions to Mineralogy and Petrology*, *94*, 42–45.

Fyfe, W. S. (1976), Chemical aspects of rock deformation, *Roy. Sbc. London Phil. Trans. Ser.*, *A 283*, 221–8.

Ganino, C., N. T. Arndt, M.-F. Zhou, F. Gallard, and C. Chauvel (2008), Interaction of magma with sedimentary wall rock and magnetite ore genesis in the Panzhihua mafic intrusion, SW China, *Miner. Deposita*, *43*, 677–694.

Gaul, O. F., W. L. Griffin, S. Y. O'Reilly, and N. J. Pearson (2000), Mapping olivine composition in the lithospheric mantle, *Earth and Planetary Science Letters*, *182*, 223–235.

Geology and Mineral Resource Bureau of Sichuan Province (1991), *The Regional Geology of Xizhang*, Geological Publishing House, Beijing (in Chinese).

Ghiorso, M. S. and R. O. Sack (1995), Chemical mass transfer in magmatic processes. IV. A revised and internally consistent thermodynamic model for the interpolation and extrapolation of liquid-solid equilibria in magmatic systems at elevated temperatures and pressures, *Contributions to Mineralogy and Petrology*, *119*, 197–212.

Harney, D. M. W., R. K. W. Merkle and G. von Gruenewaldt (1990), Platinum-group element behavior in the lower part of the Upper Zone, Eastern Bushveld Complex—Implications for the formation of the main magnetite layer, *Econ. Geol.*, *85*, 1777–1789.

Hunter, R. H. and R. S. J. Sparks (1987), The differentiation of the Skaergaard intrusion, *Contributions to Mineralogy and Petrology*, *95*, 451–461.

Hunter, R. H. and R. S. J. Sparks (1990), The differentiation of the Skaergaard intrusion, *Contributions to Mineralogy and Petrology*, *104*, 248–251.

Ionov, D. A., W. L. Griffin and S. Y. O'Reilly (1997), Volatile-bearing minerals and lithophile trace elements in the upper mantle, *Chem. Geol.*, *141*, 153–184.

Irvine, T.N. (1977), Origin of chromite layers in the Muskox intrusion and other stratiform intrusions: A new interpretation, *Geology*, *5*, 273–277.

Irvine, T. N. and M. R. Sharpe (1986), Magma mixing and the origin of stratiform oxide ore layers in the Bushveld and Stillwater Complexes. in Metallogeny of basic and ultrabasic rocks, edited by Gallagher, M.J., R. Ixer, C.R. Neary and H. M. Prichard, pp. 183–198, Institution of Mining and Metallurgy, London.

Irvine, T. N. (1987), Layering and related structures in the Duke Island and Skaergaard intrusions: Similarities, differences, and origins. *In*: Origins of Igneous Layering, edited by I. Parsons, pp. 185–245, D. Reidel Publ. Co., Dordrecht.

Jones, J. H. (1995), Experimental trace element partitioning, in *Rock Physics and Phase Relations*, *A Handbook of Physical Constants*, *Reference Shelf 3*, pp. 73–104, American Geophysical Union, Washington, DC..

Kamenetsky, V. S., S.-L., Chung, M. B. Kamenetsky and D. V. Kuzmin (2012), Picrites from the Emeishan Large Igneous Province, SW China: A compositional continuum in primitive magmas and their respective mantle sources, *J. Petrol.*, *53*, 2095–2113.

Klemm, D. D., J. Henckel, R. Dehm and G. von Gruenewaldt (1985), The geochemistry of titanomagnetite in magnetite layers and their host rocks of the eastern Bushveld Complex, *Econ. Geol.*, *80*, 1075–1088.

Liang, Q and D. C. Gregoire (2000), Determination of trace elements in twenty six Chinese geochemistry reference materials by inductively coupled plasma-mass spectrometry, *Geostandards Newsletter-The Journal of Geostandards and Geoanalysis*, *24*(1), 51–63.

McBirney, A. R. (1989), The Skaergaard layered series: I. Structure and average compositions, *J. Petrol.*, *30*, 363–97.

McBimey, A.R. and R. H. Hunter (1995), The cumulate paradigm reconsidered, *Journal of Geology*, *103*, 114–22.

Mondal, S. K. and E. A. Mathez (2007), Origin of the UG2 chromitite layer, Bushveld Complex, *J. Petrol.*, *48*, 495–510.

Morse, S. A. (1990), The differentiation of the Skaergaard intrusion. A discussion of R. H. Hunter and R. S. J. Sparks (Contrib. Mineral. Petrol. 95: 451–461), *Contributions to Mineralogy and Petrology*, *104*, 240–244.

Naldrett, A. J., A. Wilson, K. Kinnaird, M. Yudovskaya and G. Chunnett (2012), The origin of chromitites and related PGE mineralization in the Bushveld Complex: New mineralogical and petrological constraints, *Miner. Deposita*, *47*, 209–232.

Namur O., B. Charlier, M. J. Toplis, M. D. Higgins, J.-P. Liégeois and J. V. Auwera (2010), Crystallization sequence and magma chamber processes in the ferrobasaltic Sept Iles layered intrusion, Canada, *J. Petrol.*, *51*, 1203–1236.

Namur, O. B. Charlier, C. Pirard, J. Hermann, J.-P. Liégeois and J. V. Auwera (2011), Anorthosite formation by plagioclase flotation in ferrobasalt and implications for the lunar crust, *Geochim. Cosmochim. Acta*, *75*, 4998–5018.

Naslund, H. R. (1983), The effect of oxygen fugacity on liquid immiscibility in iron-bearing silicate melts, *Am. J. Sci.*, *283*, 1034–59.

Nielsen, R. L., L. M. Forsythea, W. E. Gallahanb and M. R. Fiskb (1994), Major- and trace-element magnetite-melt equilibria, *Chem. Geol.*, *117*, 167–191.

Nielsen, R. L. and J. S. Beard (2000), Magnetite MELT HFSE partitioning, *Chem. Geol.*, *164*, 21–34.

Nielsen, R. L. (2004), The shape and volume of the Skaergaard Intrusion, Greenland: Implications for mass balance and bulk composition, *J. Petrol.*, *45*, 507–530.

Pang, K.-N., M.-F. Zhou, D. Lindsley, D. Zhao and J. Malpas (2008a), Origin of Fe-Ti Oxide ores in mafic intrusions: Evidence from the Panzhihua Intrusion, SW China, *J. Petrol.*, *49*, 295–313.

Pang, K.-N., C. Li, M.-F. Zhou and E. M. Ripley (2008b), Abundant Fe–Ti oxide inclusions in olivine from the Panzhihua and Hongge layered intrusions, SW China: Evidence for early saturation of Fe–Ti oxides in ferrobasaltic magma, *Contributions to Mineralogy and Petrology*, *156*, 307–321.

Pang, K.-N., C. Li, M.-F. Zhou and E. M. Ripley (2009), Mineral compositional constraints on petrogenesis and oxide

ore genesis of the late Permian Panzhihua layered gabbroic intrusion, SW China, *Lithos*, *110*, 199–214.

Panxi Geological Unit (1984), Mineralization and exploration forecasting of V-Ti magnetite deposits in the Panzhihua-Xichang Region.

Paster, T., D. Shauwecker and L. A. Haskin (1974), The behavior of some trace elements during solidification of the Skaergaard layered series, *Geochim. Cosmochim. Acta*, *38*, 1549–1577.

Philpotts, A. R. and C. D. Doyle (1983), Effect of magma oxidation state on the extent of silicate liquid immiscibility in a tholeiitic basalt, *Am. J. Sci.*, *283*, 967–86.

Philpotts, A. R. (1982), Compositions of immiscible liquids in volcanic rocks, *Contributions to Mineralogy and Petrology*, *80*, 201–218.

Qi, L. and M.-F. Zhou (2008), Platinum-group elemental and Sr-Nd-Os isotopic geochemistry of Permian Emeishan flood basalts in Guizhou Province, SW China, *Chem. Geol.*, *248*, 83–103.

Reynolds, I. M. (1985), The nature and origin of titaniferous magnetite-rich layers in the Upper Zone of the Bushveld Complex: A review and synthesis, *Econ. Geol.*, *80*, 1089–1108.

Schock, H. H. (1979), Distribution of rare-earth and other trace elements in magnetites, *Chem. Geol.*, *26*, 119–133.

Shellnutt, J. G. and M.-F. Zhou (2007), Permian peralkaline, peraluminous and metaluminous A-type granites in the Panxi district, SW China: Their relationship to the Emeishan mantle plume, *Chem. Geol. 243*, 286–316.

Snyder, D., I. S. E. Carmichael and R.A. Wiebe (1993), Experimental study of liquid evolution in an Fe-rich, layered mafic intrusion: Constraints of Fe-Ti oxide precipitation on the *T*-f_{O2}, and *T*-*p* paths of tholeiitic magmas, *Contributions to Mineralogy and Petrology*, *113*, 73–86

Snyder, D. and S. Tait (1995), Replenishment of magma chambers: Comparison of fluid-mechanic experiments with field relations, *Contributions to Mineralogy and Petrology*, *122*, 230–240.

Song, X.-Y., R.-Z. Ma and Y.-L. Wang (1994), The characteristics of layering and magma evolution of Panzhihua intrusion, *Journal of Mineralogy and Petrology*, *14*, 37–45 (in Chinese with English abstract),

Song, X.-Y., M.-F. Zhou, Z.-Q. Hou, Z.-M. Cao, Y.-L. Wang and Y.-G. Li (2001), Geochemical constraints on the mantle source of the Upper Permian Emeishan continental flood basalts, Southwestern China, *International Geology Review*, *43*, 213–225.

Song, X.-Y., M.-F. Zhou, Z.-M. Cao, M. Sun, and Y.-L. Wang (2003), Ni–Cu–(PGE) magmatic sulfide deposits in the Yangliuping area, Permian Emeishan igneous province, SW China, *Miner. Deposita*, *38*, 831–843.

Song, X.-Y., M.-F. Zhou, Z.-M. Cao, and P.T. Robinson (2004), Late Permian rifting of the South China Craton caused by the Emeishan mantle plume, *Journal of Geology Society, London*, *161*, 773–781.

Song X.-Y., H. Zhong, M.-F. Zhou and Y. Tao (2005a), Magmatic sulfide deposits in the Permian Emeishan Large Igneous Province, SW China. in Mineral Deposit Research: Meeting the Global Challenge (the 8th Biennial SGA Meeting in Beijing) Volume 1, edited by Mao J.W. and F. P. Bierlein, pp. 465–468, Springer Berlin, Heidelberg, New York (ISBN-10).

Song, X.-Y., C.-J. Zhang, R.-Z. Hu, H. Zhong, M.-F. Zhou, R.-Z. Ma and Y.-G. Li (2005b), Genetic links of magmatic deposits in the Emeishan large igneous province with dynamics of mantle plume, *Journal of Mineralogy and Petrology*, *25*, 35–44 (in Chinese with English abstract),

Song, X.-Y., M.-F. Zhou, Y. Tao, and J.-F. Xiao (2008a), Controls on the metal compositions of magmatic sulfide deposits in the Emeishan large igneous province, SW China, *Chem. Geol.*, *253*, 38–49.

Song, X.-Y., H.-W. Qi, P. T. Robinson, M.-F. Zhou, Z.-M. Cao, and L.-M. Chen (2008b), Melting of the subcontinental lithospheric mantle by the Emeishan mantle plume; evidence from the basal alkaline basalts in Dongchuan, Yunnan, southwestern China, *Lithos*, *100*, 93–111.

Song, X.-Y., R. R. Keays, X. Long, H.-W. Qi and I. C. hlenfeld (2009), Platinum-group element geochemistry of the continental flood basalts in the central Emeisihan Large Igneous Province, SW China, *Chem. Geol.*, *262*, 246–261.

Sun, S.-S. and W. F. McDonough (1989), Chemical and isotopic systematics of oceanic basalts: Implications for mantle composition and processes. in *Magmatism in the Ocean Basins*, edited by Saunders, A.D. and M.J. Norry, Geological Society Special Publication *42*, 313–345.

Tegner, C., R. G. Cawthorn and F. J. Kruger (2006), Cyclicity in the main and upper zones of the Bushveld Complex, South Africa: Crystallization from a zoned magma sheet, *J. Petrol.*, *47*, 2257–2279.

Thy, P., C. E. Lesher, T. F. D. Nielsen and C. K. Brooks (2006), Experimental constraints on the Skaergaard liquid line of descent, *Lithos*, *92*, 154–180.

Toplis, M. J. and M. R. Carroll (1995), An experimental study of the influence of oxygen fugacity on Fe-Ti oxide stability, phase relations, and mineral melt equilibria in ferro-basaltic systems, *J. Petrol.*, *36*, 1137–1170.

Toplis, M. J. and M. R. Carroll (1996), Differentiation of ferro-basaltic magmas under conditions open and closed to oxygen: Implications for the Skaergaard intrusion and other natural systems, *J. Petrol.*, *57*, 837–858.

Van Tongeren, J. A. and E. A. Mathez (2012) Large-scale liquid immiscibility at the top of the Bushveld Complex, South Africa, *Geology*, *40*, 491–494.

Veksler, I. V., A. M. Dorfman, L. V. Danyushevsky, J. K. Jakosen and D. B. Dingwell (2006) Immiscible silicate liquid partition coefficients: Implications for crystal-melt element partitioning and basalt petrogenesis, *Contributions to Mineralogy and Petrology*, *152*, 685–702.

Villemant, B., H. Jaffrezic, J.-L. Joron and M. Treuil (1981), Distribution coefficients of major and trace elements; fractional crystallization in the alkali basalt series of Chaîne des Puys (Massif Central, France), *Geochim. Cosmochim. Acta*, *45*, 1997–2016.

von Gruenewaldt, G. (1993), Ilmenite-apatite enrichments in the Upper Zone of the Bushveld Complex: A major titanium-rock phosphate resource, *International Geology Review*, *35*, 987–1000.

Voordouw, R., J. Gutzmer, and N. J. Beukes (2009), Intrusive origin for Upper Group (UG1, UG2) stratiform chromitite seams in the Dwars River area, Bushveld Complex, South Africa, *Mineralogy and Petrology*, *97*, 75–94.

Wager, L. R. and G. M. Brown (1967), Layered Igneous Rocks, Freeman, San Francisco.

Watson, E. B. and T. H. Green (1981), Apatite/liquid partition coefficients for the rare earth elements and strontium, *Earth and Planetary Science Letters*, *56*, 405–421.

Wilson, M. (1989), Igneous Petrogenesis: A Global Tectonic Approach, London, Unwin Hyman Ltd, UK.

Xiao, L., Y. G. Xu, J. F. Xu, B. He, and F. Pirajno (2004), Distinct mantle sources of low-Ti and high-Ti basalts from the western Emeishan large igneous province, SW China: Implications for plume–lithosphere interaction, *Earth Planetary Science Letter*, *228*, 525–546.

Xu, Y. G., S. L. Chung, B. M. Jahn and G. Y. Wu (2001), Petrologic and geochemical constraints on the petrogenesis of Permian–Triassic Emeishan flood basalts in southwestern China, *Lithos*, *58*, 145–168.

Zhang, H., B. Zhang, Z. Zhao and T. Luo (1996), Continental crust subduction and collision along Shangdan tectonic belt of east Qinling: Evidence from Pb, Nd and Sr isotopes of granitoids, *Science of China (Series D)*, *39*, 273– 282.

Zhang, Y.-X. and Y. Luo (1988), The Panxi Rift, Geological Press, Beijing (in Chinese).

Zhang, Z.-C., J. J. Mahoney, J.-W. Mao and F.-S. Wang (2006), Geochemistry of picritic and associated basalt flows of the western Emeishan flood basalt province, China *J. Petrol.*, *47*, 1997–2019.

Zhang, X.-Q., J.-F. Zhang, P. Yuan, X.-Y. Song, J.-X. Guan and Y.-F. Deng (2011), Implications of compositions of plagioclase and olivine on the formation of the Panzhihua V-Ti magnetite deposit, Sichuan Province, *Acta Petrologica Sinica*, *27*(12), 3675–3688 (in Chinese with English abstract).

Zhong, H., Y. Yao, S. A. Prevec, A. H. Wilson, M. J. Viljoen, R. P. Viljoen and B.G. Liu (2004), Trace-element and Sr-Nd isotopic geochemistry of the PGE-bearing Xinjie layered intrusion in SW China, *Chem. Geol.*, *203*, 237–252.

Zhong, H. and W.-G. Zhu (2006), Geochronology of layered mafic intrusions from the Pan-Xi area in the Emeishan large igneous province, SW China, *Miner. Deposita*, *41*, 599–606.

Zhong, H., W.-G. Zhu, Z.-Y. Chu, D.-F. He and X.-Y. Song (2007), SHRIMP U–Pb zircon geochronology, geochemistry, and Nd–Sr isotopic study of contrasting granites in the Emeishan large igneous province, SW China, *Chem. Geol.*, *236*, 112–133.

Zhong, H., W.-G. Zhu, R.-Z. Hu, L.-W. Xie, D.-F. He, F. Liu and Z.Y. Chu (2009), Zircon U-Pb age and Sr-Nd-Hf isotope geochemistry of the Panzhihua A-type syenitic intrusion in the Emeishan large igneous province, southwest China and implications for growth of juvenile crust, *Lithos*, *110*, 109–128.

Zhou, M.-F., J. Malpas, X.-Y. Song, A. K. Kennedy, P. T. Robinson, M. Sun, C. M. Lesher and R. R. Keays (2002), A temporal link between the Emeishan large igneous province (SW China) and the end-Guadalupian mass extinction, *Earth and Planetary Science Letters*, *196*, 113–122.

Zhou M.-F., P. T. Robinson, C. M Lesher, R. R. Keays, C.-J. Zhang and J. M. Malpas (2005), Geochemistry, petrogenesis and metallogenesis of the Panzhihua Gabbroic layered intrusion and associated Fe-Ti-V oxide deposits, Sichuan Province, SW China*J. Petrol.*, *46*, 2253–2280.

Zhou, M.-F., N. T. Arndt, J. Malpas, C. Y. Wang and A. K. Kennedy (2008), Two magma series and associated ore deposit types in the Permian Emeishan large igneous province, SW China, *Lithos*, *103*, 352–368.